Report
R-24-04
December 2024

Some measurements of the ageing of a carbon steel

Jan Sarnet

SVENSK KÄRNBRÄNSLEHANTERING AB

SWEDISH NUCLEAR FUEL
AND WASTE MANAGEMENT CO

Box 3091, SE-169 03 Solna
Phone +46 8 459 84 00
skb.se

SVENSK KÄRNBRÄNSLEHANTERING

ISSN 1402-3091
SKB R-24-04
ID 1985677
December 2024

Some measurements of the ageing of a carbon steel

Jan Sarnet, Svensk Kärnbränslehantering AB

This report is published on www.skb.se

Summary

The tensile testing results in this report show that static strain ageing increases with the amount of pre-strain and ageing temperature for the carbon steel EN 1.0562. The static strain ageing increases the yield strength noticeably, but no increase in tensile strength and no decrease in ductility can be determined. The steel possibly over-age judging from the slightly decreasing yield strengths for longer holding times. In addition, the testing at elevated temperatures shows that dynamic strain ageing and the decrease of the ductility is only apparent at 200–300 °C, and such temperatures are not foreseeable in the repository. Consequently, strain ageing can be neglected in the mechanical analyses of the canister.

Sammanfattning

Dragprovningstesterna i denna rapport visar att statisk deformationsåldring ökar med mängden deformation och åldringstemperatur för kolstålet EN 1.0562. Den statiska deformationsåldringen höjer sträckgränsen märkbart, men ingen ökning av draghållfastheten och ingen minskning av duktiliteten kan fastställas. Möjligtvis överåldras stålet att döma av de minskande sträckgränserna vid längre åldringstider. Dessutom visar dragprovning vid förhöjd temperatur att dynamisk töjningsåldring och minskning av duktiliteten endast är uppenbar vid 200–300 °C och dessa temperaturer är inte förutsebara i slutförvaret. Därför kan åldring försummas i mekaniska analyser av kapseln.

Contents

1 Introduction

The load carrying capacity of metals and alloys as structural steels, increases with work-hardening and the addition of alloying elements, but such strengthening can reduce the ability of the metal to deform without breaking. On the other hand, smaller grain size increases the strength often with retained ductility, especially at sizes below 0.1 millimetre (100 microns).

If alloying elements or solute atoms are mobile, they can lock further deformation and therefore strengthen the material. Such interactions result in marked yield points and some associated loss of ductility, either after the deformation; static strain ageing, or during the deformation; dynamic strain ageing. The phenomena, commonly referred to as simply “strain ageing”, are common in iron and steels (Hultgren 1966, Honeycombe 1968, 2017 with Bhadeshia), Bergström and Roberts (1971), Kocks et al. (1975). The strain ageing effects on steel properties and behaviour in nuclear applications have been further investigated by Hänninen et al. (2001), Seifert and Ritter (2005), and Rao et al. (2021).

The KBS-3 canister for geological storage of spent nuclear fuel consists of a copper shell and a cast iron insert. Its mechanical integrity is analysed in Jonsson et al. (2018). Alternative designs of the insert have been considered and the purpose of the present document is to assess strain ageing behaviour of a canister with a steel insert. This document presents information and some knowledge on the ageing of pressure vessel steels and of SKB’s nodular cast iron in Section 2. Properties relevant to strain ageing of test manufactured canister insert components of low-alloyed steel are presented in Section 3 and are compared to the corresponding properties of SKB’s nodular cast iron in Section 4. Based on this comparison, a preliminary assessment of ageing of the low-alloyed steel components are made in Section 5. A tensile testing design of experiments to gain further knowledge of ageing of the steel components is presented in Section 6. Results of such tensile tests are presented in Section 7. A discussion of the issues addressed in this document is provided in Section 8 along with conclusions regarding the significance of strain ageing for the low-alloyed steels considered in an alternative design of SKB’s canister insert.

2 Characteristics of ageing

The strain ageing of a ferritic material can be identified by tensile testing at elevated temperatures or by pre-deformation at room temperatures, storing, and retesting after some elapsed time (Brindley and Barnby 1966). Dynamic strain ageing materials will show small serrations in the stress-strain curve, as in the stress-strain curve at 300 °C in Figure 2-1 and they are in the literature referred to as the Portevin-Le Chatelier (1923) effect (PLC). The dynamic strain ageing will result in a reduced strain to fracture (elongation).

The locking of dislocations by ageing is particularly strong when solute atoms in the material are small and mobile. For example, carbon and nitrogen atoms are small enough to fit between the iron atoms of ferritic iron and steels and distort the crystal lattice. By diffusion to atomic crystal defects (dislocations), formed by previous deformation, locally increased concentrations lock dislocations increasing the stress of further deformation. This behaviour is known as static strain ageing. In addition, due to the high mobility at temperatures around 100–300 °C, these small atoms can diffuse to the moving dislocations during deformation, known as dynamic strain ageing (Honeycombe 1968). The diffusion of nitrogen was measured and described by Wert (1950) and Figure 2-2 shows how the measured diffusivity increases with increasing temperature. Nitrogen and carbon are the most dominating solutes in strain ageing (Kocks et al. 1975, p 223, Bhadeshia and Honeycombe 2017). Brindley and Barney (1966) investigated the effect of nitrogen and Caillard recently (2016) demonstrated the effect of carbon on strain ageing of mild steels. Dieter (1988) argues that nitrogen is more important for strain ageing because of its higher solubility and diffusion coefficient, and also for its lower tendency to form precipitation during cooling.

The static strain ageing materials will show a marked upper yield point followed by a serrated yield plateau of reduced flow stress (Zhao et al. 2012). In addition, the specimens also show a reduced elongation.

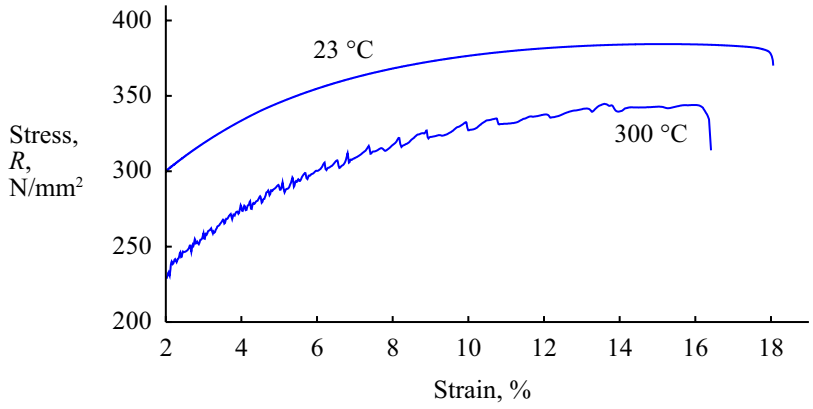

Figure 2-1. *Nodular cast iron tensile test curves without signs of strain ageing at 23 °C and with serrations at 300 °C (Sarnet 2022).*

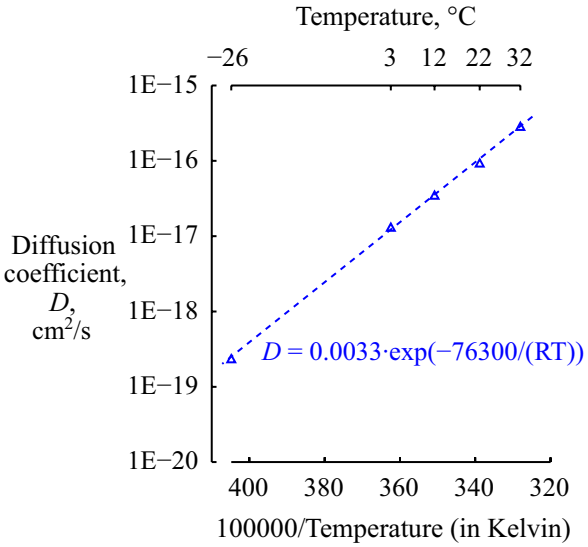

Figure 2-2. *The temperature dependence of nitrogen diffusion in iron, data from Wert (1950).*

2.1 Dynamic strain ageing of pressure vessel steels

The strain ageing of steel partly depends on the nitrogen content of ferritic steels (Brindley and Barnby 1966). Those authors studied the effect of nitrogen by disregarding carbon through a precipitation heat treatment. Later, Otterberg and Karlsson (1979) showed that an A533 grade B pressure vessel steel exhibited a raised ultimate tensile strength and therefore strain age at 200–300 °C when using a strain rate of about 0.0001 s^{-1}. No stress-strain curves were presented but they reported that the dynamic strain ageing occurs at lower temperatures for lower strain rates. The relative susceptibility to dynamic strain ageing has recently been evaluated for four low alloy steels used in the nuclear applications by Rao et al. (2021). The 22 NiMoCr 3 7, 20 MnMoNi 5 5, 508, and 533 steels all have similar alloying content. The steels were tempered and showed yield points at room temperature tensile testing. Since several combinations of temperature and strain rate were analysed, the dynamic strain ageing covariation between the temperature and strain rate is evident from Figure 2-3. In the figure, the crosses show combinations for which serrations are detectable and dynamic strain ageing occurs. The triangles show combinations with upper yield points. The dashes show combinations of temperatures and strain rates with no apparent dynamic strain ageing. An activation energy Q could be calculated for the occurrence of dynamic strain ageing in that the slope of $\log_{10}$(strain rate) versus 100 000/T[in Kelvin] is set as Q/R, where R is the universal gas constant. From that data, the activation energy for dynamic strain ageing is calculated to 80 kJ/mol.

The activation energy is similar to energies reported for pressure vessel steel by Otterberg and Karlsson at 84 kJ/mol and by Jana et al. (2018) at 93 kJ/mol.

The ranking by Rao et al. (2021) of the resistance to strain ageing was based on ductility behaviour at 23–400 °C. The ageing effect on ultimate tensile strength and ductility, measured as area reduction at tensile testing, was moderate. The strongest strain ageing effect coincided with the highest solute nitrogen content at 110 ppm. But at 60–80 ppm nitrogen, strain ageing brittleness are both present and absent depending on steel grade or its properties. As shown in Table 2-1, the two steels SA533 grade B and 20 MnMoNi 5 5 show a decrease in ductility, and on the other hand, the 22 NiMoC 3 7 shows no decrease in ductility.

Table 2-1. Chemical compositions of four steel grades and their relative decrease in ductility due to dynamic strain ageing. In weight-percent if not stated otherwise (Rao et al. 2021).

Steel grade	C	Si	Mn	P	S	Ni	Cr	Mo	Cu	Al	Ceq	N (ppm)	Relative area reduction (%)
22 NiMoCr 3 7	0.22	0.20	0.91	0.008	0.007	0.88	0.42	0.53	0.04	0.018	0.44	80	0.6
SA 508 grade 3	0.21	0.27	0.69	0.004	0.004	0.78	0.38	0.63	0.16	0.015	0.42	110	16.4
20 MnMoNi 5 5	0.21	0.25	1.26	0.004	0.004	0.77	0.15	0.50	0.06	0.013	0.50	70	12.3
SA 533 grade B	0.25	0.24	1.42	0.006	0.018	0.62	0.12	0.54	0.15	0.030	0.57	60	8.9

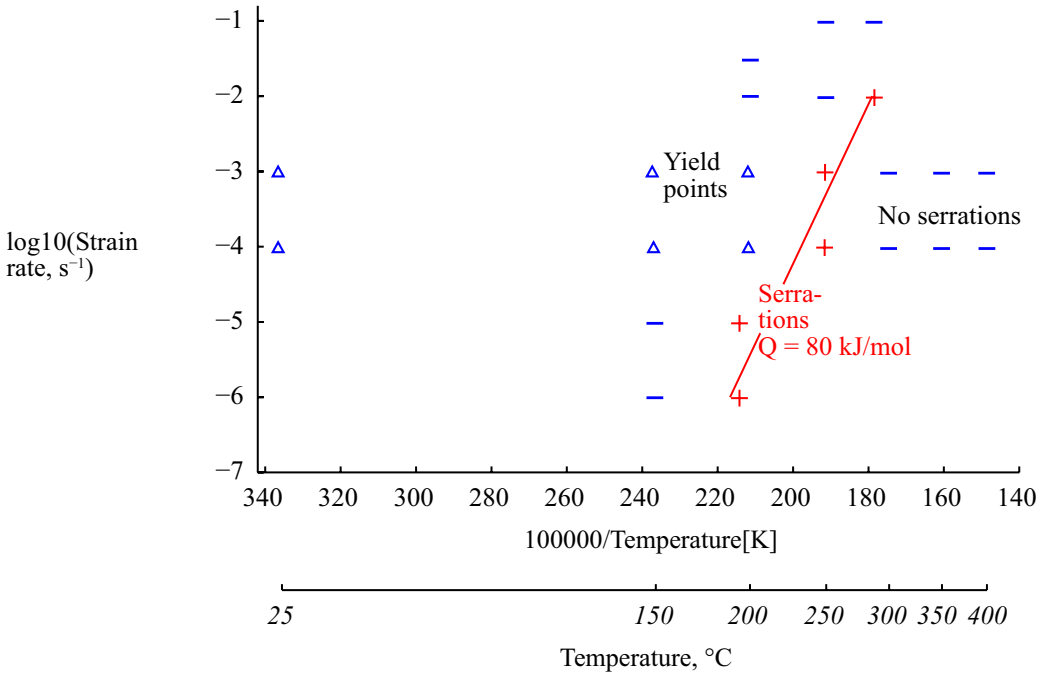

Figure 2-3. *The occurrence of dynamic strain ageing for a pressure steel. Data from Rao et al. (2021).*

In addition, Wang et al. (2012) identified serrations at 200 °C at 10^{-3} s^{-1} and marked yield points at 20 °C for a carbon-manganese steel. Further measurements on such a C-Mn steel were analysed by Ren et al. (2017) who showed a strain-rate dependence of the frequency and size of the serrations as well as the dependence of the occurrence of serrations on strain-rate. Ren et al. only presented observations of serrations for one tensile testing temperature although at nine strain rates, making analysis of the covariation between temperature and strain rate impossible. Table 2-2 also shows that the serration amplitude increases with decreasing strain rates. It is noted that the results, ranging from logarithmic strain rates of −5 to −1.5, agree with the measurements by Rao et al. (2021), plotted in Figure 2-3, as they fall on the left side of the red demarcation line. Table 2-2 also shows that, at 200 °C, the serrations start almost immediately in the range 0.00005–0.0004 s^{-1}, but for lower and higher strain-rates it appears that some finite critical strain is needed before the serrations and the Portevin-Le Chatelier effects are detectable from the stress-strain curves.

Table 2-2. Strain ageing critical strain and serration amplitude for a C-Mn-steel tested at 200 °C. Interpreted from Ren et al. (2017).

Strain rate (s^{-1})	Critical strain (%)	Serration amplitude (N/mm^2)
0.000010	3.9	7
0.000017	1.5	6
0.000050	0.8	5
0.00010	0.7	4
0.00040	0.7	3
0.0010	1.2	2
0.0040	1.8	1.5
0.01	2.3	1.3
0.03	8.7	0.8

2.2 Static strain ageing of two pressure vessel steels

The static strain ageing of an A533B pressure vessel steel was investigated by Otterberg and Karlsson (1979) and an A737 grade C pressure vessel steel was investigated by Sekizawa (1981). The chemical compositions are given in Table 2-3.

Table 2-3. Chemical composition, in weight percent (Fe-balance), of two pressure vessel steels.

Grade	C	Mn	Si	S	P	Ni	Mo	N
A533B	0.21	1.48	0.25	0.002	0.008	0.65	0.53	0.009
A737C	0.18	1.29	0.30	0.007	0.005	0.15	0.08	0.016

The pre-deformation was 4 % in the investigation by Otterberg and Karlsson, and 2 %, 5 %, and 10 % in the investigation by Sekizawa. A pre-deformation up to 5 % and an ageing treatment at 200–300 °C raise the yield strength and the ultimate tensile strength. From the results by Sekizawa it seems that additional increase of pre-strain and ageing temperatures will not further increase the strength.

2.3 Ageing of SKB's nodular cast iron

Some recent measurements of dynamic and static ageing of nodular cast iron have been made independently by Pihlajamäki (2017) and Björklund et al. (2024). To compare with those measurements, SKB investigated the quench ageing (ageing occurring as a material cools after heat treatment), dynamic strain ageing, and static ageing for two nodular cast iron inserts (Sarnet 2022). The two inserts of the SKB investigation differ slightly in composition, foremost in silicon and carbon content. In general, higher silicon and carbon content reduce the ductility.

Serrations of the stress-strain curves indicate dynamic strain ageing. For the cast iron tested at standard testing rate, dynamic strain ageing is only visible at the right side of Figure 2-4 for the temperatures 300 °C and 400 °C.

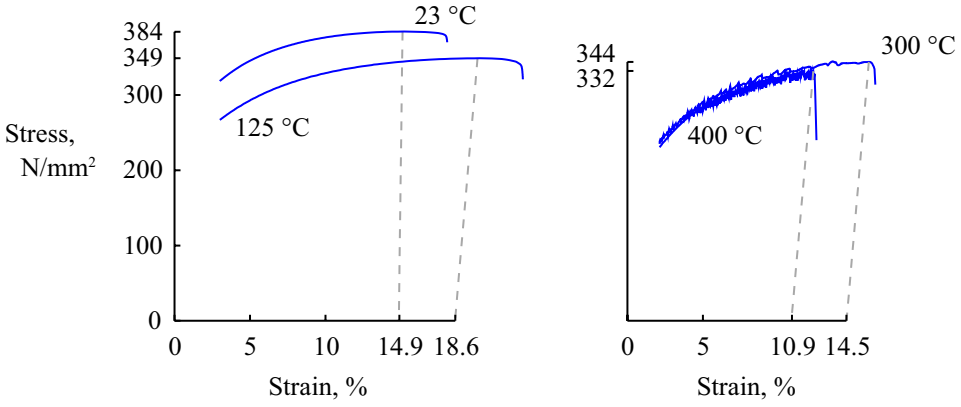

Figure 2-4. *Stress-strain curves of ferritic nodular cast iron at different tensile testing temperatures (Sarnet 2022).*

3 Properties of cylinders ST1, ST2, ST3

The alternative steel insert is a hollow cylinder approximately 1 m in diameter and 5 m long. The wall thickness is approximately 80 mm. Recently, SKB has procured three open die forged, hollow cylinders (tubes) to evaluate such an alternative insert design. The material, EN 1.0562, is a carbon non-alloy steel formulated for hot forming, such as rolling or open die forging, into plate, cylinder or other components. The condition is usually normalized from an additional heating, resulting in a phase transformation from austenite to ferrite during cooling. 1.0562 is the EN numeric designation of this material whereas P355N is the EN chemical designation.

As a result of the hot working, forming and normalizing heat treatment, the microstructure can be fine-grained with a grain size down to 0.02 mm. Further, porosity from the cast (ingot) will be consolidated through local shearing during the hot working, an effect depending on the relative geometry during the hot working. The efficiency of the defect consolidation will be improved by an increased relative contact length to workpiece thickness, an increased working bite (Vater and Heil 1971). The fine grain size and low amount of porosity will contribute to the material's high yield stress, ultimate tensile strength, and ductility.

The P355N hollow cylinders (tubes) ST1, ST2, and ST3 were formed by open die forging of ingots at high temperature, with the final grain size set, either by direct cooling, or by an additional normalizing heat treatment. The chemical compositions of the tubes are shown in Table 3-1. The last two tubes were forged from one, heavier ingot. The carbon content and calculated carbon equivalent are the same for the two ingots and three tubes, although there are slight differences in composition.

Table 3-1. Chemical compositions of three hollow cylinders (tubes). In weight-percent, except for oxygen and hydrogen which are given in ppm by weight.

Cylinder	C	Mn	Si	P	S	Cr	Ni	Mo	Al	Cu	V	Ti	N	O	H	Ceq
ST1	0.15	1.22	0.19	0.005	0.004	0.08	0.09	0.08	0.021	0.09	0.05	0.001	0.014	24	1.2	0.42
ST2/ST3	0.15	1.28	0.16	0.008	0.0011	0.12	0.14	0.05	0.029	0.16	0.05	0.001	0.008	16	1.7	0.43

The tensile stress-strain curve of an ST1 specimen, Figure 3-1 shows an upper yield point R_{eH}, at 395 N/mm^2, a yield plateau with lower yield point, R_{eL}, 344 N/mm^2, and an ultimate tensile strength, R_m, at 474 N/mm^2. The yield plateau is also called Lüders deformation (François et al. 1998, p. 198). The marked upper yield point occurs at 0.1–0.2 % strains and the yield plateau is up to 1.5–2 % strains, respectively, are also shown in Figure 3-1. Higher ultimate tensile strength coincides with higher content of manganese, phosphorus, sulphur, chromium, copper, and hydrogen. Also, higher ultimate tensile strength coincides with lower content of silicon, molybdenum and nitrogen. The upper yield point results from locking of deformation by solute atoms such as carbon and nitrogen. Figure 3-1 shows that the steel has a good ductility.

Figure 3-2 shows that the measured ultimate tensile strengths are in line with the standard values of 450–590 N/mm^2 for the material of 65–100 mm thickness (SS-EN 10216-3:2013). The variation is quite small within each steel cylinder, but there can be some systematic differences, within and between cylinders, due to processing parameters and differences in chemical composition. Figure 3-2 shows that the measurements of ultimate tensile strength is higher for cylinders ST2 and ST3 having been forged from the same ingot compared to ST1 forged from another ingot. Secondly, Figure 3-2 shows that the strength varies within the wall thickness. The tensile strength at mid-wall positions are lower than for outer and inner wall positions for ST2 and ST3. It can be reasoned that the strengths of the latter positions are favoured by faster cooling and higher working during forging of the hollow cylinders (tubes), leading to a finer microstructure with less microdefects, and similarly, that they are favoured by a faster cooling during the normalizing heat treatment, also leading to a finer microstructure.

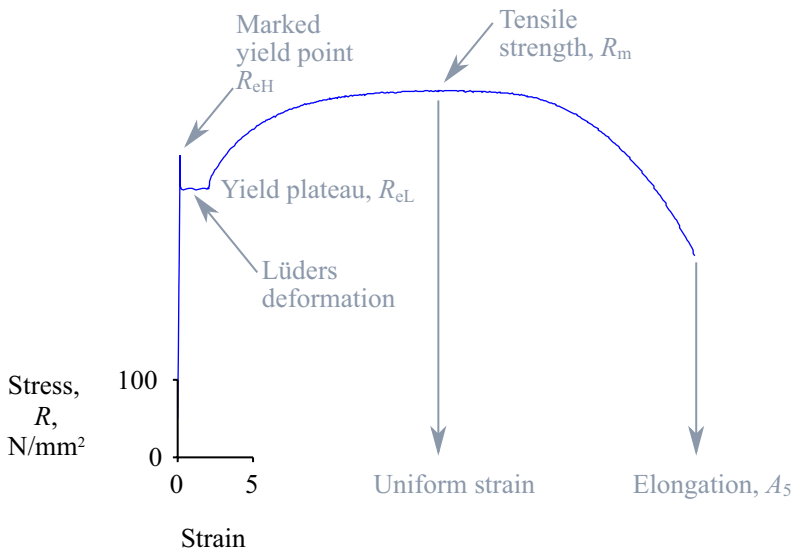

Figure 3-1. *Tensile stress-strain curve of the carbon steel P355N, cylinder ST1, tensile specimen 21911.*

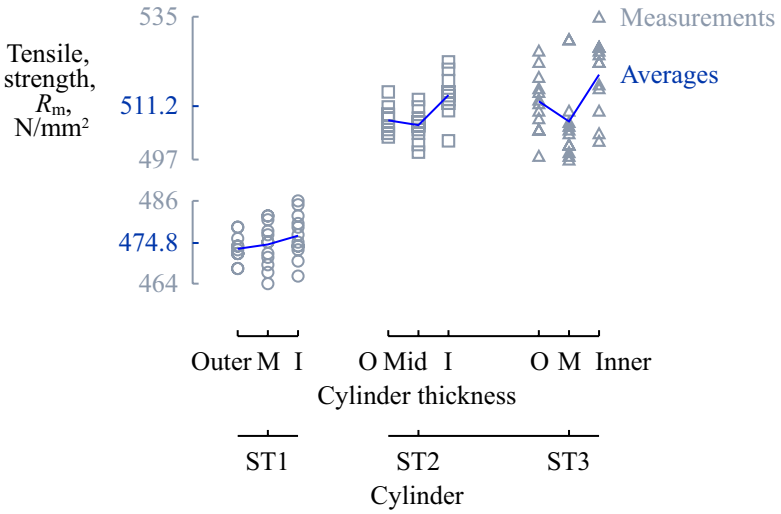

Figure 3-2. *Tensile strength measurements[1,2,3,4] (pencil grey symbols) and averages (ink blue lines) of the three cylinders ST1, ST2, and ST3 for three radial positions in the cylinder wall.*

[1] SKBdoc 1958695 ver 1.0 (Internal document.)

[2] SKBdoc 1965338 ver 1.0. (Internal document.)

[3] SKBdoc 1970174 ver 2.0. (Internal document.)

[4] SKBdoc 1975273 ver 1.0. (Internal document.)

Figure 3-3 and 3-4 show the tensile strength, R_m, and elongation, A_5, against ASTM grain-size class, respectively. A small jitter has been added to the grain size to increase the differentiation of the scatter points. As seen, ST2/ST3 has higher tensile strength despite coarser grain size (lower size class) which is a bit surprising. An explanation could be the higher content of Cr and Ni and differences in microstructure. For elongation, the difference is quite small between the groups, with the softer material displaying the largest elongation.

The ductility of the steel cylinder, measured as the elongation, A_5, is in average 33 % and higher than, for example, of nodular cast iron, 12 % given by the standard (SS-EN 1563:2018), and of test manufactured nodular cast iron inserts, 13.7 % and 17.4 % in average (Sarnet 2022, Figure 4-3 and Table 4-6). The uniform strain (not shown here) is lower and comparable to the values of cast iron. The variation of the ductility is low for the steel cylinders. A three-sigma interval of the elongation, A_5, for the steel cylinders is around 25–36 %.

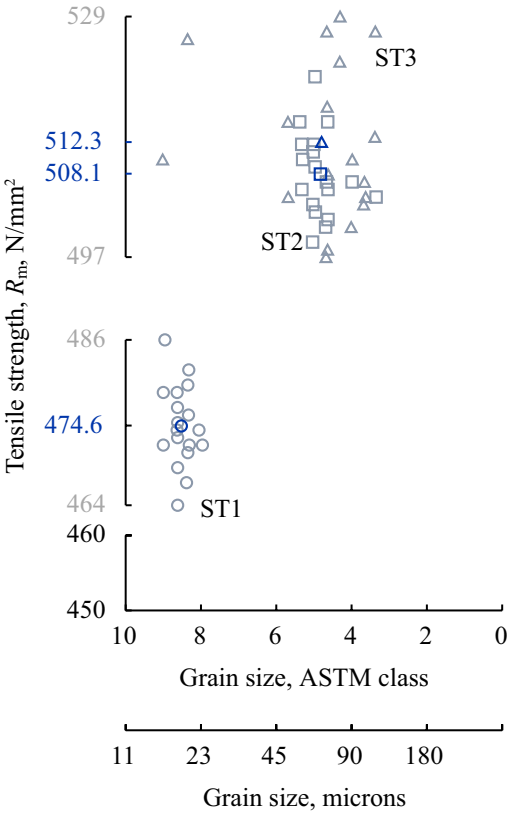

Figure 3-3. *The tensile strength[1,2,3,4] plotted against the grain size class according to ASTM E112-13.*

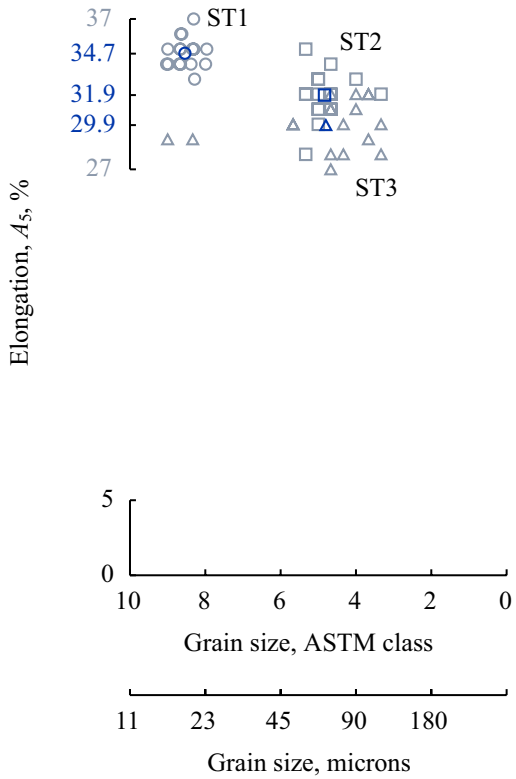

Figure 3-4. *The elongation at failure[1,2,3,4] plotted against the grain size class according to ASTM E112-13.*

4 Comparison of nodular cast irons and carbon steels

The carbon steel and the nodular cast iron have some similarities in that they are both ferritic metals. The chemical compositions differ, as shown in Table 4-1, in that the content of carbon and silicon are higher in the cast iron. Most of the carbon in the cast iron is precipitated as nodular graphite whereas the silicon is in solution and strengthens the ferritic matrix. On the other hand, the manganese content is higher in the steel. Other notable differences are the lower nitrogen content and higher hydrogen content of the cast iron.

The matrix structure of the cast iron is ferrite and the matrix structure of the P355N is ferrite with islands of pearlite.

Table 4-1. Chemical compositions of the cast iron insert i76 and the low-alloy steel cylinder ST1. In weight-percent if not stated otherwise.

Materials		C	Si	Mn	P	S	Ni	N (ppm)	H (ppm)
Cast iron	400-15	3.5	2.3	0.17	0.02	0.05	0.4	40	3.0
Steel	P355N	0.15	0.16	1.28	0.008	0.001	0.14	80	1.05

The microstructures differ between the ferritic nodular cast iron and the low-alloy carbon steels, and also between the steel cylinders ST1 and ST3, as shown in Figures 4-1, 4-2 and 4-3. Comparison between the last two figures shows that the microstructure is coarser in cylinder ST3 than in ST1. In Figure 4-3 areas with pearlite are visible in between the (white) ferrite.

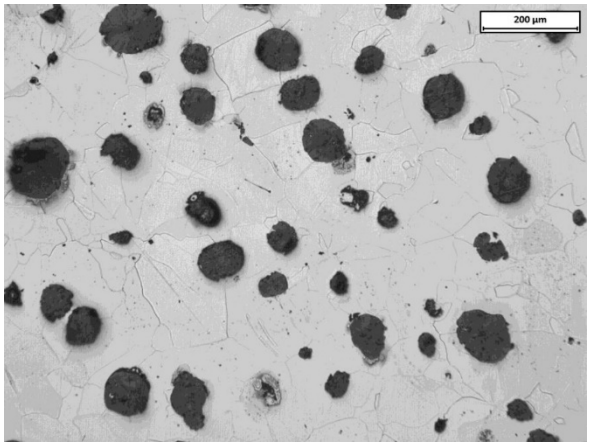

Figure 4-1. *Nodular cast iron microstructure insert i76.*

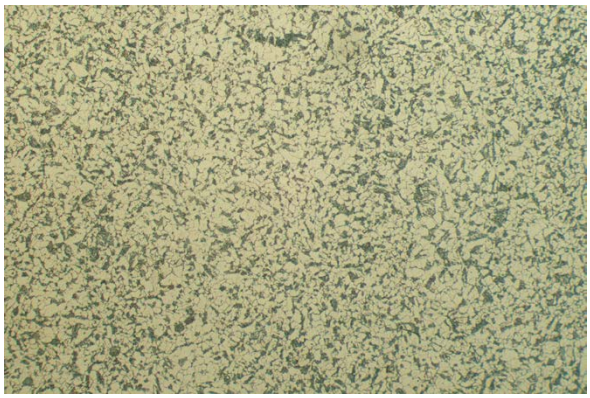

Figure 4-2. *P355N steel microstructure. ST1, sample TA03. 100×.*

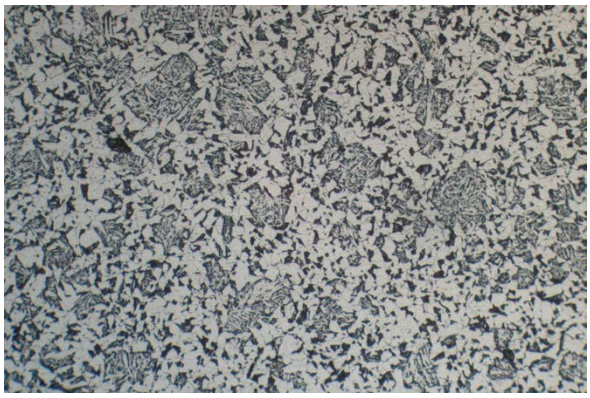

Figure 4-3. *P355N steel microstructure. ST3, sample TA05. 100×.*

The steel cylinders have a marked yield stress and a yield plateau which are typical of low alloyed steels. The cast iron shows no such effect in the as-cast condition. Compare Figure 4-4, where the start of the tensile curves, up to 3 % strain, is shown, and where a nodular cast iron exhibits a soft transition between the elastic and plastic part of the curve. The P355 steel on the other hand shows marked upper yield point and a sudden decrease and a yield plateau for 1.5 % of strain.

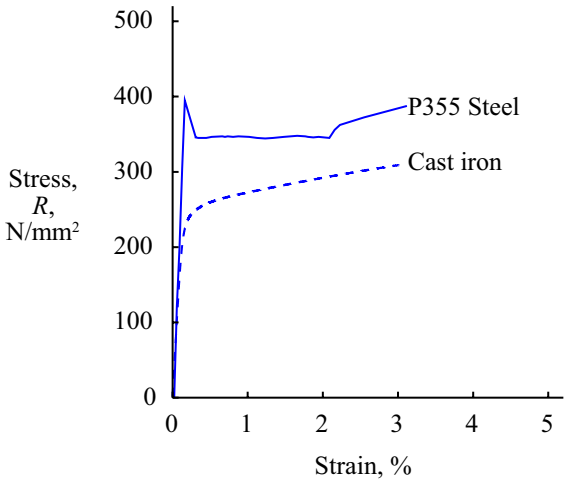

Figure 4-4. *Comparison of the yielding of the P355N steel of ST1 and of nodular cast iron.*

5 Preliminary assessment of the strain ageing of the low alloyed steels P355N

The insert could in theory be subjected to a shear load in the proposed repository. It is interesting to evaluate if dynamic strain ageing could occur during such shearing, and if static strain ageing could occur after such shearing.

5.1 Dynamic strain ageing

During an improbable deformation by an earthquake with shearing at 1 m/s, the deformed thickness would be in the size of 100 mm. The strain rate would be high (1 m/s)/(100 mm) = 10 s^{-1}. Such rate would raise the temperature slightly, but more importantly shift the dynamic strain-ageing to higher temperature.

The temperature increase can be calculated as the product of the average flow stress 400 N/mm^2, and the strain 3 %, divided by the product of the density 7 800 kg/m^3 and the specific heat 500 $J \cdot kg^{-1} \cdot K^{-1}$ (Hensel & Spittel 1978, Richardson et al. 1985). This yields a temperature increase of 400 000 000 × 0.03/(7 800 × 500) = 3 K.

The steel cylinders have tensile properties and deformation behaviour, such as upper yield strength and a yield plateau, typical for metals exhibiting static strain ageing. Still, at room temperature tensile testing, they show a good ductility of 30 % elongation and good toughness. This is interpreted as a good resilience to dynamic strain ageing embrittlement for the steel cylinders.

5.2 Static strain ageing

The investigated cylinders are supposed to be in a normalized and annealed state. Therefore, no remaining pre-deformation is expected in the material.

The temperature evolution of the insert over time in the final repository is assumed to be as in Figure 5-1 and reported by Ikonen (2020). Diffusion or boundary dependent processes could occur in the ferritic insert material. The diffusion of nitrogen can be calculated by integrating the diffusion coefficient as a function of temperature with respect to time. A temperature dependent nitrogen diffusivity from Wert (1950) was used. The integration of the diffusivity with respect to time was calculated with 24 steps, with temperatures from Figure 5-1, yielding a diffusion distance for nitrogen of √0.0002 cm = 0.14 mm. This means that nitrogen can diffuse through a ferritic grain, to the adjacent grain boundaries with surrounding ferritic grains, and into the neighbouring grains; the grains having sizes of 0.020–0.080 mm in a ferritic insert.

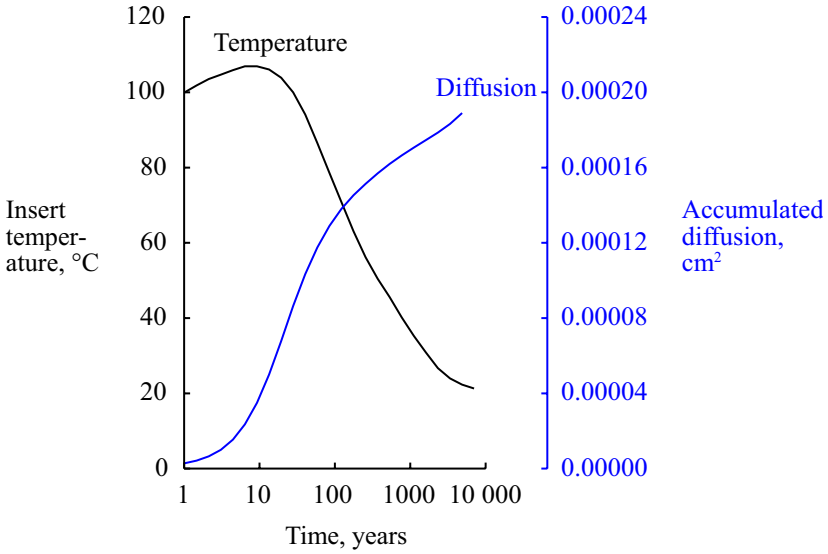

Figure 5-1. *The temperature evolution of the insert (black solid line) Ikonen (2020) and a calculated squared diffusion distance of nitrogen.*

6 Design of ageing experiment

Strain ageing can reduce the ductility and toughness of steels. To evaluate the loss of ductility and toughness of P355N steel cylinders, new ageing experiments are presented in this report. For those experiments some additional testing of tensile samples from the cylinders ST1 and ST3 were performed.

Much is known about strain ageing. The main influencing factors are temperature and strain rate for dynamic strain ageing, and temperature and (ageing) time for static strain ageing. To evaluate the variation caused by other factors, as steel composition and microstructure, and the supposed annealing in the final repository, a structured, reduced design of the experiments was used to determine an efficient combination of factors in the tensile testing runs (Box et al. 2005, Bergman et al. 2017).

The insert will be subjected to decay heat from the spent fuel elements in the repository. The temperatures are low, below 115 °C, but will prevail for some hundreds of years (Renström 2020). In the experiments, the time influence from decay heat had to be simulated by increased temperatures. The acceleration was calculated with Wert's diffusional measurements of nitrogen in (ferritic) iron (Wert 1950).

A marked yield stress and the presence of a yield plateau are indications of static strain ageing. The upper yield stress and the elongation zone might also be changed with additional heat treatment during manufacturing or stress-relieving processes in a final repository. It would be important to evaluate the as-received state (of microstructure), heat-treated states, or heat affected. These will be levels "as-received", "stress-relieved" and (sub-critically) "process annealed" in the design of experiments and Figure 6-1 shows the temperature interval for such treatments in the iron-carbon phase diagram according to Phragmén given in Hultgren et al. (1943).

To separate the effect of manufacturing (metallurgical) influences from strain ageing, some of the tensile specimens in the experiment were stress-relieved or process annealed before tensile testing for strain ageing. The metallurgical state of the cylinder samples is normalised condition. An approximate third of the specimens were stress-relieved at 500 °C for 30 hours which gives a diffusion distance of nitrogen of $\sqrt{0.0026}$ cm = 0.5 mm according to diffusivities measured by Wert (1950). A further third were subcritically annealed at 650 °C for 4 hours, also giving a 0.5 mm diffusion distance. The rest of the specimens was tested in as-received state.

The chemical composition cannot be changed readily, except for the variation between ST1 and ST3.

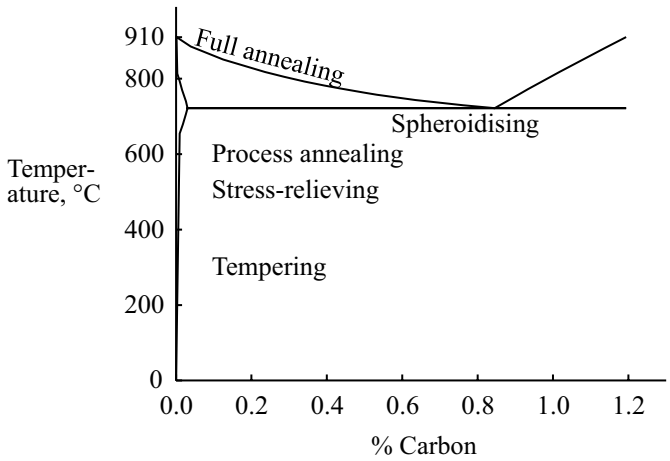

Figure 6-1. *Iron-rich corner of the iron-carbon equilibrium phase diagram (Hultgren et al. 1943) with approximate temperatures for heat treatments (Hultgren et al. 1943, Rowe 1977). Redrawn by the present author.*

6.1 Tensile testing

The tensile testing was performed using a Zwick-Roell machine. The maximum load cell force was 100 kN. The pre-deformation for the static strain ageing experiments was performed at 23 °C and with the deformation rate 0.00025 s^{-1}. There was no pre-deformation for the dynamic strain ageing tests.

6.2 Dynamic ageing experiments

To evaluate the dynamic strain ageing effect on ductility and indirectly on toughness, tensile testing was performed at elevated temperatures. Visible qualitative dynamic strain ageing by serrations in the stress-strain curve, and possible quantitative reductions in ductility are analysed in Section 7.5.

For dynamic strain ageing, the main affecting factors are temperature, strain rate and chemical composition of the steel. Temperatures at which dynamic strain ageing are known to occur are generally 100–300 °C in iron (Honeycombe 1968) and specifically 180–300 °C in steel (Rao et al. 2021).

Since strain ageing is controlled by thermal release (Honeycombe 1968, p. 150, Kocks et al. 1975, p. 129), it is reasonable to arrange the design of experiments as a function of 1/temperature in Kelvin. For practical reasons the strain rates were chosen to coincide with rates in the tensile testing standards (SS-EN-ISO-6892-1, SS-EN-ISO-6892-2).

In Figure 6-2 combinations of strain rate and temperature for the testing of occurrence of dynamic strain ageing are shown. The occurrence of dynamic strain ageing demonstrated by Jana et al. (2018) and Rao et al. (2021) for low alloy steel is shown with grey crosses. The fitted line in grey representing the maximum dynamic strain ageing effect. The slope of the fitted curve can be used to calculate the activation energy for the dynamic strain ageing process.

First, a full factorial design of experiments was considered. The main factors, 5 temperatures × 5 strain rates and would give 25 tensile tests. Other factors that might influence the results would be additionally 3 states × 2 cylinders × 3 wall thickness positions and result in 450 runs for a full design. It is supposed that microstructure and composition are only marginally affected by the state, cylinder and wall-thickness position, and therefore their combinations are reduced, yielding a 25-run experiment. The factor “axial position” is disregarded based upon the small influence on mechanical properties.

However, even the reduced design of experiments was further slimmed down to 9 tensile tests, seen as red squares in Figure 6-2, due to the lack of specimens, and the declination by the laboratory to test at the strain rates of 0.1/s and 0.01/s.

Table 6-1. Block 1 Experiments for dynamic strain ageing, ST1 and ST3.

Run	Temperature (°C)	Strain rate (s^{-1})	State	Cylinder	Wall thickness
103	250	0.002	Annealed	ST1	Inner
106	275	0.00025	As-received	ST3	Outer
108	275	0.002	Stress-relieved	ST3	Mid
115	220	0.002	Stress-relieved	ST1	Inner
117	220	0.00025	Stress-relieved	ST3	Outer
118	195	0.00025	As-received	ST1	Mid
119	255	0.00007	Stress-relieved	ST1	Inner
120	180	0.00007	Annealed	ST3	Outer
122	285	0.00007	As-received	ST3	Mid

The cylinders ST1 and ST3 were of steel grade P355N and were available for the experimental runs. The design of experiments provided a screening of the temperature-strain rate interplay on the dynamic strain ageing, but it will not give the possibility for determination of the activation energies for dynamic strain ageing and other stress – strain rate processes. The total number for dynamic strain ageing experiments was 9 runs, as seen in Table 6-1.

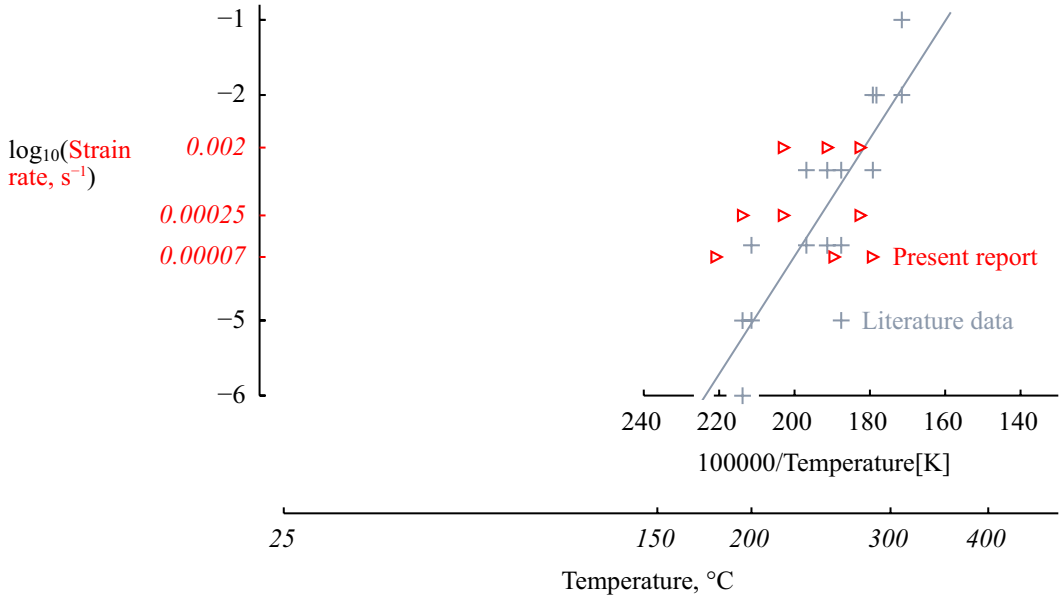

Figure 6-2. *Proposed levels of strain rates and temperatures, as red triangles for experiments, on dynamic strain ageing for ST1 and ST3. Based on data from Rao et al. (2021) and Jana et al. (2018), as grey crosses. For the red triangles, the strain rate, rather than its logarithm, was given on the y-axis.*

6.3 Static ageing experiment

For static strain ageing, the main affecting factors were pre-strain, ageing temperature, ageing time, and chemical composition of the steel. The ageing time is an easy-to-change factor, whereas pre-strain, and ageing temperature are hard to change factors.

A full factorial design of experiments would be 3 strains × 3 ageing temperatures × 3 ageing times × 3 states × 2 cylinders = 162 runs. A reduced design consisting of 18 runs can be seen in Table 6-2. The design of the 18-run experiment was built in the software Statistica.

Table 6-2. Reduced design of experiments for static ageing.

Run	Pre-strain (%)	Temperature (°C)	Time (h)	State	Cylinder	Wall thickness
301	1	20	50	Annealed	ST3	Mid
303	0.3	20	50	Stress relieved	ST1	Inner
304	1	75	16	Stress relieved	ST3	Mid
305	1	155	5	As-received	ST3	Mid
308	1	155	50	Stress relieved	ST1	Outer
309	3	155	16	Annealed	ST1	Outer
312	1	20	5	Annealed	ST1	Outer
313	3	75	50	Annealed	ST1	Mid
314	0.3	20	5	Annealed	ST3	Outer
316	3	155	5	Stress relieved	ST3	Inner
317	0.3	155	16	As-received	ST1	Mid
318	3	155	16	Annealed	ST3	Inner
321	0.3	75	5	Stress relieved	ST1	Inner
322	0.3	75	50	As-received	ST3	Outer
323	0.3	20	16	Stress relieved	ST3	Outer
324	3	75	50	As-received	ST3	Inner
325	3	20	16	Stress relieved	ST1	Mid
327	1	75	5	As-received	ST1	Inner

6.4 Factors and responses

In summary, the factors, grouping or categorical variables, were strain rate, deformation and ageing temperature, annealing, and microstructure and chemical composition between and within cylinders. The responses, dependent variables, were yield stresses, extent of the yield plateau, tensile strengths, the smoothness of the stress-strain curve and elongation.

The influence on strain ageing from chemical compositions, including the amounts of nitrogen, oxygen and hydrogen, the microstructure, and the grain size was not investigated.

7 Results

The mechanical properties after the ageing trials have been compiled and analysed in this chapter, and are compared to the initial properties. Both the effects of static and of dynamic ageing on yield strength, tensile strength, ductility, and the visual appearance of the tensile curves have been accounted for.

The mechanical properties, measured at inner, mid and outer wall positions, varied systematically between ST1 and ST3 before the ageing trials, where ST3 had higher tensile strength. In addition, there was a small difference in tensile strength before the ageing trials for different radial position in wall thickness, where tensile specimens from the inner and/or outer wall positions had higher tensile strengths.

7.1 Tensile strength

According to Table 7-1 the specimen tensile strength varies between the two cylinders and was lower during dynamic ageing. The possible influencing factors on the strength were cylinder identity, radial position in cylinder wall, top and bottom of the cylinder, temperature before and during testing. From the averages in Table 7-1 and Figure 7-1, it is obvious that the difference in strength between cylinder ST3 and ST1 was retained after the strain ageing test.

Table 7-1. Tensile strength, cylinders ST1 and ST3.

			Tensile strength, R_m (N/mm^2)											
			Initial				Ageing						Averages	
							Static			Dynamic				
ST1	Outer	Bottom	472	473			478	481	482				475.1	468.5
		Topp			468	472								
	Mid	B	471	481									467.4	
		T			464	475	468	469	475	436				
	Inner	B	475	482			421	477	486	438	455	469	464.7	
		T			470	474								
ST3	Outer	B	513	523			507	523	535	493	514	516	513.2	513.7
		T			498	510								
	Mid	B	529	529									502.8	
		T			497	499	480	503	507	476	505			
	Inner	B	523	535			526	533	538				528.3	
		T			517	526								
Averages			494.8				493.8			478.0			491.5	

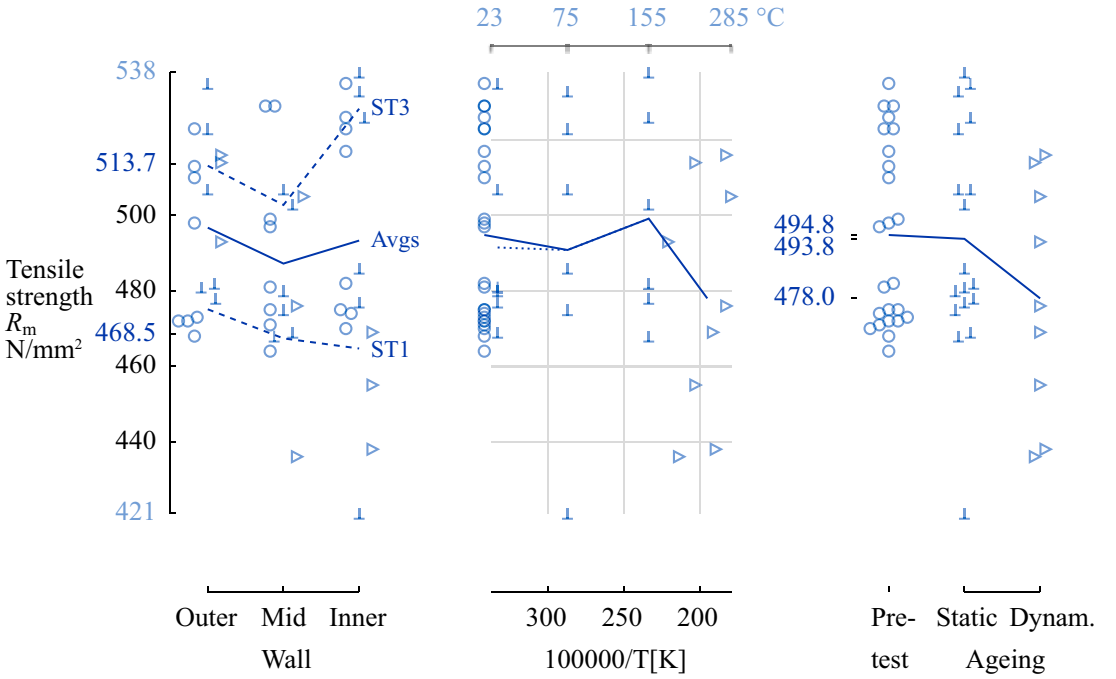

Figure 7-1. *Strain ageing specimen tensile strength measurements and averages versus level combinations of wall positions, reciprocal temperature, and test types with, other factors marked with symbols. Inspired from a template in Bergman et al. (2017, p 43).*

Systematic tensile strength differences between the cylinders (ST1/ST3) could be statistically ensured with Analysis of Variance, ANOVA, (Blom and Holmquist 1998, Box et al. 2005). Radial positions in the cylinder wall (Outer, mid, and inner) could almost be statistically ensured in the same analysis. In such variance analysis, the total squared variation around the mean value of the tensile strength, 38 749 $(N/mm^2)^2$, was partitioned into components. According to the second column of Table 7-2, the analysis gave a partitioning into components corresponding to test, cylinder, wall radial position, height, the interactions, and a residual error. The factors *Type of test, cylinder, and height* have statistically significant influence on the tensile strength and have been marked in red in Table 7-2. Contributions to the variation from other factors are included in the residual root mean square sum of 173 $(N/mm^2)^2$ which gives an internal variation and standard deviation of 13.16 N/mm^2. Due to oversight on the part of the author, not all combinations of factors were represented in the tensile test specimens available in the design of the experiment. At each level of a factor, all levels of every other factor are not represented in Table 7-1 as they should in a proper Latin square design (sw. romerska kvadrater) (Box et al. 2005, pp 157–160, Bergman 1992, p 101). For example, the static ageing tests did not include outer and inner wall specimens at top (axial) position. Therefore, the variation between the bottom and top of the cylinder cannot be analysed as a result of the ageing.

Table 7-2. Analysis of Variance (ANOVA) table for specimen tensile strength in N/mm² for the ageing experiments.

Source of variation	Sum of squares	Degrees of freedom	Mean squares	Ratio of mean square (F)	Significance probability (p)	Comment
Test (pre, static, dynamic)	2005	2	1002	5.79	0.008	(**) significance
Cylinder	26670	1	26670	153.91	0.000	(***) significance
Radial position in cylin. wall	1029	2	514	2.97	0.067	almost significance
Height	1243	1	1243	7.17	0.012	(*) significance
Test × Cylinder	221	2	111	0.64	0.535	no significance
Test × Wall	324	4	81	0.47	0.759	no significance
Cylinder × Wall	1149	2	574	3.31	0.051	almost significance
Cylinder × Height	538	1	538	3.10	0.089	almost significance
Wall × Height	167	2	83	0.48	0.623	no significance
Test × Cylinder × Wall	239	2	120	0.69	0.509	no significance
Cylinder × Wall × Height	139	2	69	0.40	0.674	no significance
Error	5025	29	173	-		√173.3 = 13.16
Total	38749	50	775.0			√775 = 27.84

The standard deviation √173.3 = 13.16 N/mm² is a measure of variation after correcting for the influence of the type of strain ageing test, cylinder, radial position in cylinder wall, height position, and the interaction between the two. This variation has contributions both from the difference in composition, working, and cooling. It could be a conservative measure of the accuracy in tensile strength of the specimens, 13.16/492.4 N/mm²/N/mm² = 2.7 %.

To highlight and describe variations in measurements, so-called normal distribution diagrams (plots) can be constructed and drawn. As an example, consider the tensile strength given for ST1 in Table 7-3. First, the measured values were ordered by size and then the two variables y and z are calculated as indicated in Table 7-3 where Φ is the distribution function of the standard normal distribution (Blom and Holmquist 1998, pp 74–75, Box et al. 2005, pp 33–34). Instead of the classic calculation of the probability $y_i = (i-1/2)/n$ in those references, the present author calculated $y_i = (i-1/3)/(n+1/3)$ in line with the Statistica software.

Table 7-3. Measured tensile strength of specimens from cylinders ST1.

Number, i	Tensile strength ST1 (N/mm²)	$y_i = (i-1/3)/(n+1/3)$, $n = 13$	$z_i = \Phi^{-1}(y_i)$
1	421*	0.05	−1.645
2	436	0.125	−1.150
3	438	0.2	−0.842
4	455	0.275	−0.598
5	468	0.35	−0.385
6	469	0.425	−0.189
7	469	0.5	0
8	475	0.575	0.189
9	477	0.65	0.385
10	478	0.725	0.598
11	481	0.8	0.842
12	482	0.875	1.150
13	486	0.95	1.645

* No stress-strain data recorded after 3 percent strain.

The measurements x_i were plotted against $y_i = (i - 1/3)/(n + 1/3)$ and $z_i = \Phi^{-1}(y_i)$, $i = 1, 2, \ldots, n = 13$, as in Figure 7-2. The scale on the left vertical axis is linear in z. In Excel, z, can be calculated with the function NORM.S.INV. As can be seen, the plotted measurement points adhere well to straight lines, at least for the 14 specimens from cylinder ST3. This means that reasonable statistical descriptions and models for the variation within test cylinder ST3 could be given by a normal distribution.

The arithmetic mean of the 13 tensile strength measurements for ST1 was 464.2 N/mm^2 and the standard deviation is 20.5 N/mm^2. The corresponding numerical values for ST3 were 511.1 and 19.3, respectively. The values determine the parameters in fitted normal distributions that become the ink blue lines in Figure 7-2. The two-sigma limits for the diameter of cylinder ST1 are 423.2 and 505.2, defining the normal distribution line. Similarly, two-sigma limits for ST3 are 472.6 and 549.7. The slopes of the lines are determined by the spread, standard deviation, within the sample positions, the smaller the spread, the steeper the slope. In Figure 7-2, the lowest measured tensile strength at 421 N/mm^2 from cylinder ST1 is an outlier of the distribution, and is even smaller than the lower two-sigma limit for ST1. According to the testing report (Nilsson 2024) that value is due to a malfunction during testing and could be removed from the distribution. However, no replacement specimen was available at the time of testing, and only 12 values can be plotted in a normal plot for ST1.

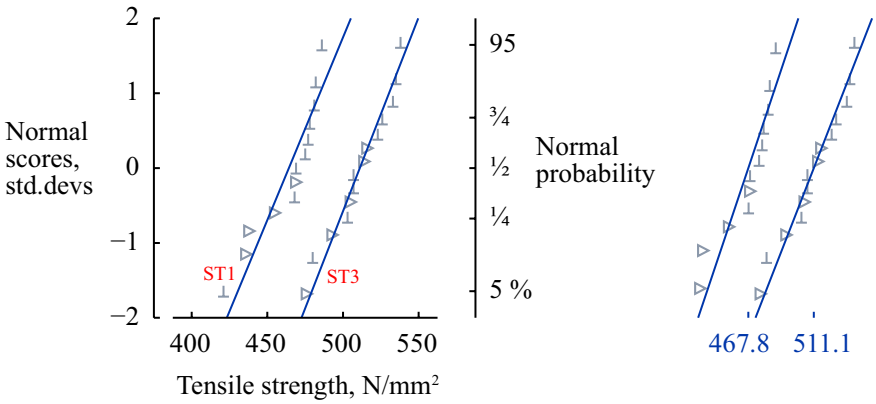

Figure 7-2. *Normal probability plots of the tensile strengths from cylinders ST1 and ST3.*

7.2 Influence of tensile testing laboratories

The tensile properties reported in Section 3 were tested for cylinders ST1, ST2, and ST3 in the years 2021–2022 at a laboratory hereafter labelled laboratory 5. Using additional samples from the three cylinders, strain ageing tensile testing was performed in 2023 at another laboratory, hereafter labelled laboratory 3. As it was assumed that there should be no differences between the laboratories, no tensile specimens were tested to fracture before strain ageing at laboratory 3.

Unlike the ultimate tensile strength and elongation, the upper and lower yield strengths were measured before strain ageing. Therefore, it was possible to compare the results of the upper and lower yield strength reported by the two laboratories labelled 5 and 3. Only tangential specimens, from top and bottom of the cylinders ST1 and ST3, and in the as-received state were compared. This reduced the number of comparable yield strength values from laboratory 3, to only 5 measurements.

As expected, the measurements of upper and lower yield strengths differ for the two hollow cylinders ST1 and ST3 according to the Analysis of variance shown in Tables 7-5 and 7-7, and Figure 7-4. Surprisingly, as in seen Table 7-4, the reported upper yield strength, R_{eH}, differs considerably, by 17 MPa or by 4 %, between the two laboratories. The upper yield strength was higher as measured by laboratory 3 during 2023. The cause is unknown.

Table 7-4. Upper tensile yield strength for the static strain ageing experiments.

		R_{eH} (N/mm^2)							
		Laboratory 5			Laboratory 3				
		Wall position			Wall position				
Cylinder	Axial position	Outer	Mid	Inner	Outer	Mid	Inner	Averages	
ST1	Top	390 384	399 377	392 390		404		390.9	394.9
	Bottom	395 388	396 395	399 402			418	399.0	
ST3	Top	400 388	391 372	399 401		402		393.3	408.2
	Bottom	437 427	410 426	401 412	427		430	421.3	
Averages		398.8			416.2			401.8	

The result of a variance analysis in Table 7-5 shows that both the cylinder and the laboratory have a significant influence on the upper tensile yield strength.

Table 7-5. Analysis of Variance (ANOVA) table for upper tensile yield strength for the static strain ageing experiments.

Source of variation	Sum of squares	Degrees of Freedom	Mean squares	Ratio of mean square (F)	Significance probability (p)	Comment
Cylinder	1 275	1	1 275	6.64	0.016	(*) significant
Lab. 5 / 3	1 076	1	1 076	5.60	0.026	(*) significant
Cylinder × Labs.	19.51	1	19.51	0.10	0.753	not significant
Error	4 804	25	192.1	-		√192.1 = 13.9
Total	7 175	28	256.2			√256.2 = 16.0

Table 7-6. Lower tensile yield strength for the static strain ageing experiments.

		R_{eL} (N/mm^2)							
		Laboratory 5			Laboratory 3				
		Wall position			Wall position				
Cylinder	Axial position	Outer	Mid	Inner	Outer	Mid	Inner	Averages	
ST1	Top	337 338	344 334	345 340		*335*		339.0	344.5
	Bottom	345 343	351 342	357 352			*360*	350.0	
ST3	Top	349 368	350 345	367 382		354		359.3	373.4
	Bottom	366 384	391 390	389 390	*380*		396	385.8	
Averages			358.3			365.0		359.4	

The numbers in italic font in Table 7-6 were read out, or extrapolated, by the present author from the original data files since they were missing in the original laboratory report (Nilsson 2024).

As can be seen from the variance analysis scheme in Table 7-7, no systematic differences of lower tensile yield strength could be demonstrated for the laboratories.

Table 7-7. Analysis of Variance (ANOVA) table for lower tensile yield strength for the static strain ageing experiments.

Source of variation	Sum of squares	Degrees of Freedom	Mean squares	Ratio of mean square (F)	Significance probability (p)	Comment
Cylinder	6048	1	6048	29.89	0.000	(***) significant
Lab. 5/3	60.68	1	60.68	0.30	0.589	not significant
Cylinder × Labs.	0.3403	1	0.3403	0.0017	0.968	not significant
Error	5058	25	202.3	-		√202.3 = 14.22
Total	11167	28	398.8			√399 = 19.97

The forces were high but did not exceed the load cell maximum of 100 kN (for any tensile test), and the relationship between the maximum force and the upper yield stress is plotted in Figure 7-3. The 0.95 percent prediction interval was calculated in the Statistica software and is indicated by the dashed red curves considering the uncertainties of both measurement of yield stress and force. As shown in Figure 7-3, steel grades or strain rates with an expected ultimate tensile strength higher than 560 N/mm^2 will require a smaller nominal specimen diameter.

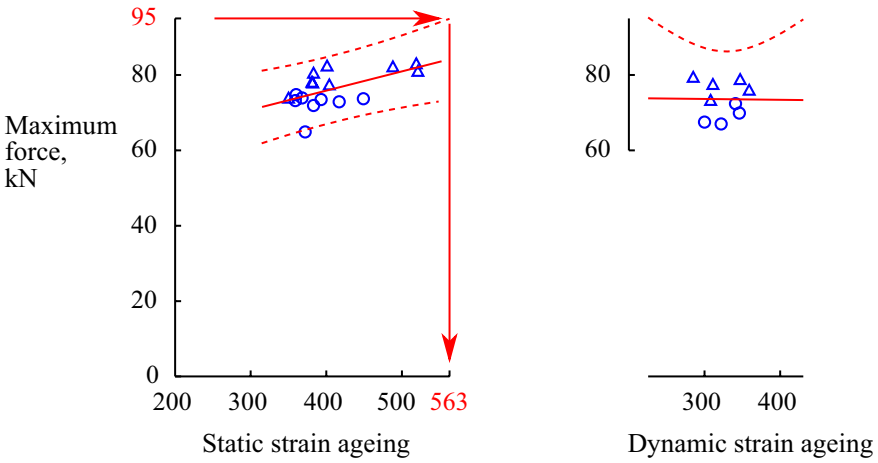

Figure 7-3. *Maximum force fitting and 0.95 prediction interval for 14 mm diameter tensile specimen.*

7.3 Effect of heat treatments on yield strength

The upper yield points at room temperature were measured during the pre-straining and in effect before the actual static strain ageing. In total, the upper yield points for 18 specimens were recorded, 9 specimens from cylinder ST1 and 9 from cylinder ST3. As a natural consequence of the finite strain in the static ageing trials, it was not possible to measure the ultimate tensile strength. The effects of heat treatments, wall thickness, and cylinder on the yield points are shown by three graphs in Figure 7-4, below. The pencil grey numbers on the ordinate scale axis are the minimum and maximum values, and the ink blue numbers are the averages for each factor. To reveal the effects the upper yield strength averages are given for combinations of factors with solid lines (Bergman et al. 2017, p 43). In addition, the symbols have been color coded to represent the metallurgical state and to some extent imitate the processing temperatures. Such fundamental use of color has been recommended by Tufte (1990, p.81). The as-received state is indicated by black symbols, the stress-relieved state by red symbols and the annealed state by orange symbols, respectively. As seen, the strength increased when the specimens had been stress-relieved or annealed, compared to the strength of the specimens in the as-received state (condition). The recorded strength values of cylinder ST3 were generally higher than those of cylinder ST1, except for two mid wall specimens, one in the as-received state and another in the annealed state.

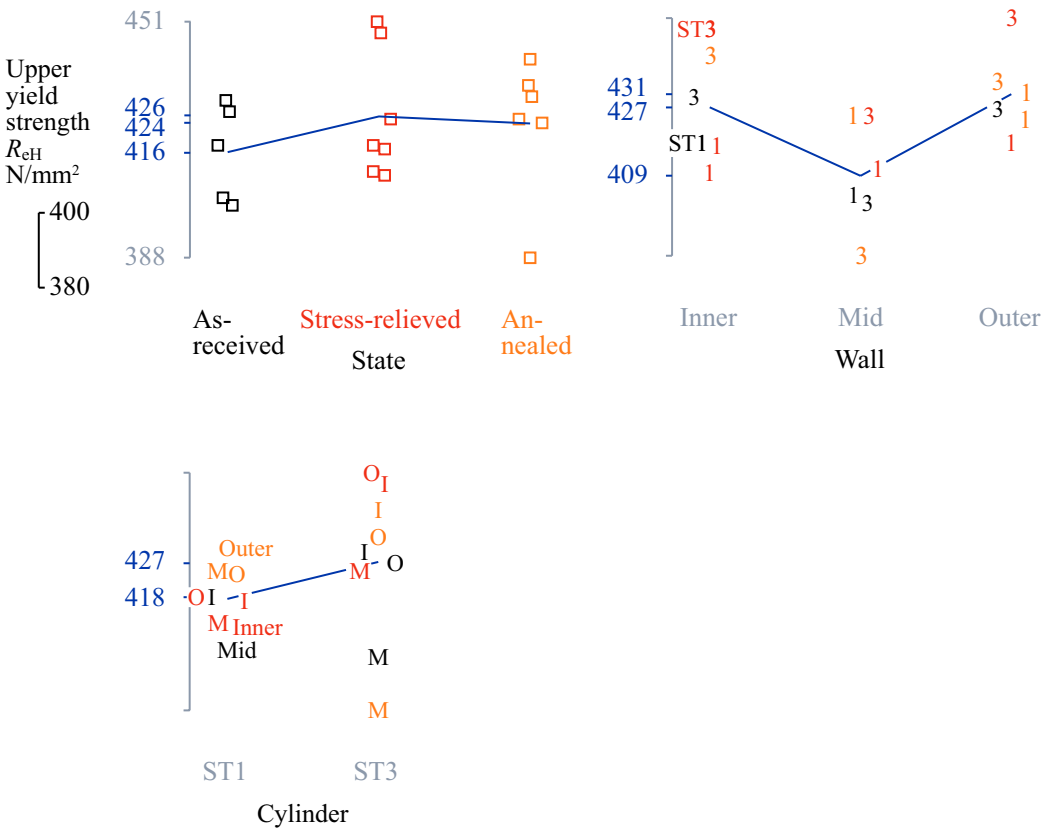

Figure 7-4. *Upper yield strength versus state, radial position in wall, and cylinder. State indicated by colors, cylinder with number, and radial wall position with text/letter.*

7.4 Static strain ageing

The static strain ageing can be evaluated as the increase of tensile strength during ageing after an initial deformation (Otterberg and Karlsson 1979). But in the present report, tensile strength reference values have not been available, and therefore the yield strength as used for the analysis instead.

In the tensile testing report (Nilsson 2024), the lower yield strength, R_{eL} during pre-strain was only given for 10 out of 18 tensile tests. The missing readings coincide with low pre-strains, mostly at the lowest level of 0.3 %, but some were also missing from pre-strains of 1.0 %. The author of the present document has evaluated the R_{eL} for the remaining 8 tensile tests from the available original data, given as italics in the second column of Table 7-8. For 8 of the 18 tests, it was possible to calculate notable increase in yield strength.

Table 7-8. Increase (rise) in lower yield stress for the static strain ageing experiments.

	Ageing			Material			R_{eL} (N/mm²)		
Run	Strain (%)	Temperature (°C)	Time (h)	Cylinder	Wall	State	Before	After	Increase
301	1.0	20	50	ST3	Mid	Annealed	*344*	349	5
303	0.3	20	50	ST1	Inner	Stress-relieved	*350*	349	−1
304	1.0	75	16	ST3	Mid	Stress-relieved	371	379	8
305	1.0	155	5	ST3	Mid	As-received	354	396	42
308	1.0	155	50	ST1	Outer	Stress-relieved	352	356	4
309	3.0	155	16	ST1	Outer	Annealed	358	434	76
312	1.0	20	5	ST1	Outer	Annealed	360	367	7
313	3.0	75	50	ST1	Mid	Annealed	359	411	52
314	0.3	20	5	ST3	Outer	Annealed	*358*	380	22
316	3.0	155	5	ST3	Inner	Stress-relieved	396	507	111
317	0.3	155	16	ST1	Mid	As-received	*335*	336	1
318	3.0	155	16	ST3	Inner	Annealed	397	500	103
321	0.3	75	5	ST1	Inner	Stress-relieved	*395*	369	−26
322	0.3	75	50	ST3	Outer	As-received	*380*	381	1
323	0.3	20	16	ST3	Outer	Stress-relieved	*393*	395	2
324	3.0	75	50	ST3	Inner	As-received	396	487	91
325	3.0	20	16	ST1	Mid	Stress-relieved	345	394	49
327	1.0	75	5	ST1	Inner	As-received	*360*	360	0

For one specimen, there was a unexpected decrease of 26 N/mm² in lower yield strength, but for the low pre-strain of 0.3 %, there was in average no significant change in yield strength, −0.2 N/mm² for the six specimens.

Otterberg and Karlsson plotted the rise in ultimate tensile strength as a function of the ageing temperature, and found an increase with temperature up to 250 °C. For the present data, without separation of strain, time and state, there was an increase in lower yield strength with increased ageing temperature as shown in Figure 7-5. When the data was plotted against the pre-strain, again without any separation of groups, the increase was even clearer. The averages are displayed as ink blue lines. There were only three ageing times, but these suggest an overageing with time. An exponential curve, red dashed line, fits the increase in yield strength versus the temperature well as expected from a general Arrhenius-equation. Ageing temperatures of 20, 95, and 155 °C might give equally spaced increase in lower yield stress.

It is clear from Figure 7-5 (at right) that for low strains only negligible static strain ageing will occur. The plastic pre-strain is shown to be the dominant factor for strain ageing to occur.

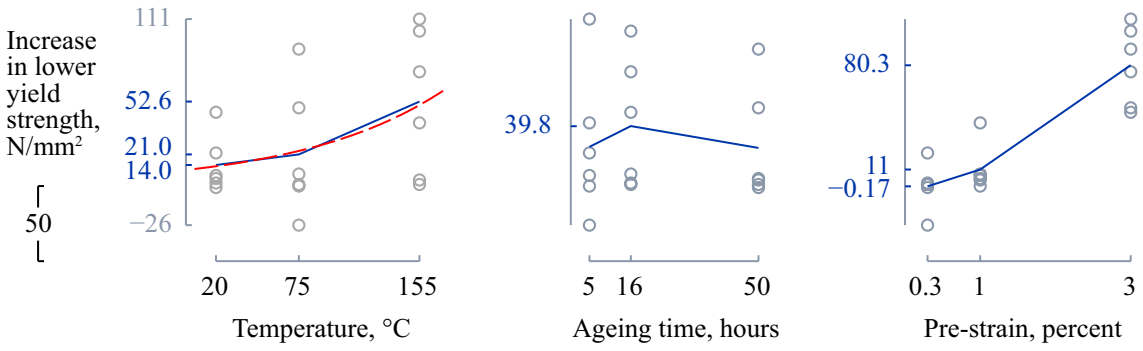

Figure 7-5. *The increase of lower yield stress versus the ageing temperature, time, and pre-strain.*

A general regression model in the statistical software Statistica was applied to the rise in the yield strength, and from the results in Table 7-9 it can be seen that the pre-strain is of statistical significance, and that increasing ageing temperature which is indicated by brighter colors in Figure 7-6 almost was statistically significant as a factor influencing the rise in yield strength. The factor cylinder also has a statistically significant impact on the increase in yield strength due to strain ageing. Figure 7-6 shows that yield strength of cylinder ST3 increases more than ST1. This was somewhat surprising since the carbon content is the same and ST3 has a lower nitrogen, oxygen, and silicon content.

Table 7-9. General Linear Model (GLM) table for lower tensile yield strength for the static strain ageing experiments combining continuous predictors as pre-strain, temperature, time, and categorical factors as cylinder, radial position in wall, and state.

Source of variation	Sum of squares	Degrees of Freedom	Mean squares	Ratio of mean square (F)	Significance probability (p)	Comment
Pre-strain	22 204.64	1	22 204.64	111.4691	0.000	(***) significant
Ageing temperature	868.02	1	868.02	4.3575	0.066	almost significant
Ageing time, in log scale	215.54	1	215.54	1.0820	0.325	not significant
Cylinder	2 916.88	1	2 916.88	14.6430	0.004	(**) significant
Wall	477.98	2	238.99	1.1997	0.345	not significant
State	78.43	2	39.21	0.1969	0.825	not significant
Error	1 792.80	9	199.20			√199.2 = 14.11
Total	28 554.28	17	1 679.66			√1 680 = 40.98

The diagrams of Figure 7-5 have been rearranged in Figure 7-6 in response to the results of the general linear model in Table 7-9. In addition, a diagram showing the influence of the cylinder was added.

Measurements of ultimate tensile strength were available for specimens from ST1 and ST3 as-received metallurgical state. Compared with measurements after static strain ageing, only a small increase can be seen in Figure 7-7. The measurements without static strain ageing were measured at laboratory 5 and the measurements subjected to static strain ageing were measured at laboratory 3 and were as-received, stress-relieved, or process annealed.

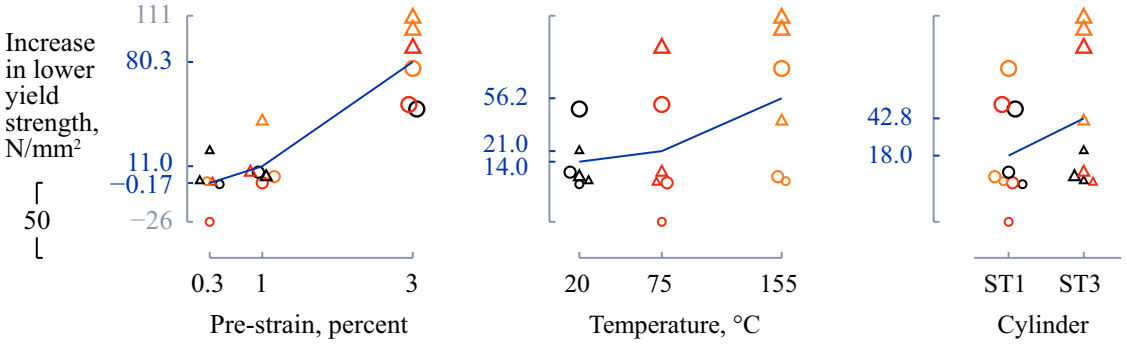

Figure 7-6. *The increase of lower yield stress versus pre-strain, ageing temperature, and cylinder, respectively.*

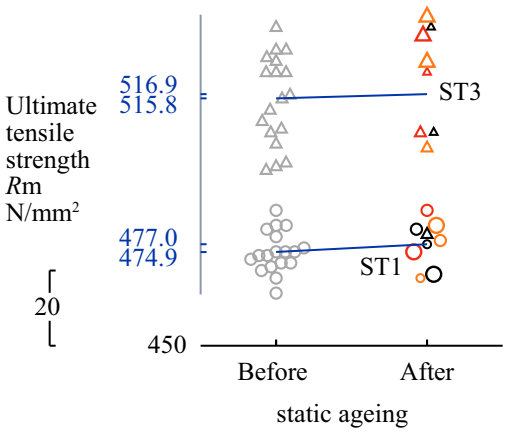

Figure 7-7. *Comparison of ultimate tensile strength before and after static strain ageing for two P355N-steel cylinders.*

In Table 7-10, the ductility after the static strain ageing, measured as the strain to fracture (elongation A_5), is given. The strain will be concentrated after the maximum stress is reached, and therefore the elongation will depend slightly on the gage length (Dieter 1988, p. 280). The gage length is 80 mm for these 14 mm diameter tensile test specimens.

The same ductility data is plotted in Figure 7-8. As seen, only a small decrease in the elongation can be seen with increased pre-strain.

Table 7-10. The ductility measured as the elongation after fracture for strain aged specimens.

Run	Strain (%)	Temperature (°C)	Time (h)	State	Cylinder	Wall	A_5 (%)
303	0.3	20	50	Stress-relieved	ST1	Inner	35.2
314	0.3	20	5	Annealed	ST3	Outer	30.7
323	0.3	20	16	Stress-relieved	ST3	Outer	20.0
321	0.3	75	5	Stress-relieved	ST1	Inner	33.6
322	0.3	75	50	As-received	ST3	Outer	35.7
317	0.3	155	16	As-received	ST1	Mid	33.0
301	1.0	20	50	Annealed	ST3	Mid	35.1
312	1.0	20	5	Annealed	ST1	Outer	26.9
304	1.0	75	16	Stress-relieved	ST3	Mid	26.3
327	1.0	75	5	As-received	ST1	Inner	32.8
305	1.0	155	5	As-received	ST3	Mid	32.3
308	1.0	155	50	Stress-relieved	ST1	Outer	31.1
325	3.0	20	16	Stress-relieved	ST1	Mid	33.4
313	3.0	75	50	Annealed	ST1	Mid	34.6
324	3.0	75	50	As-received	ST3	Inner	28.7
309	3.0	155	16	Annealed	ST1	Outer	31.8
316	3.0	155	5	Stress-relieved	ST3	Inner	25.4
318	3.0	155	16	Annealed	ST3	Inner	27.2

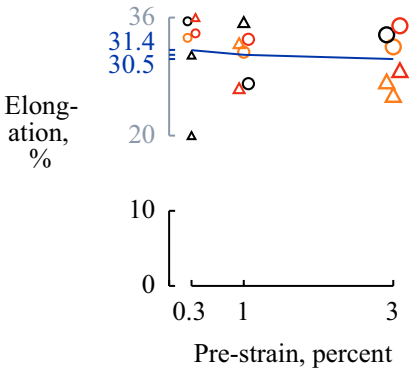

Figure 7-8. *Elongation versus the pre-strain of strain aged specimens.*

With the general linear model (GLM) in Table 7-11 no statistically significant decrease of the elongation at failure after static strain ageing can be seen for any of the tested sources of variation.

Table 7-11. General Linear Model (GLM) table for the elongation for the static strain ageing experiments combining continuous predictors as pre-strain, temperature, time, and categorical factors as cylinder, radial position in wall, and state.

Source of variation	Sum of squares	Degrees of Freedom	Mean squares	Ratio of mean square (F)	Significance probability (p)	Comment
Pre strain	3.39	1	3.39	0.221	0.650	not significant
Ageing temperature	0.01	1	0.01	0.000	0.986	not significant
Ageing time	32.34	1	32.34	2.107	0.181	not significant
Cylinder ST1/ST3	53.82	1	53.82	3.507	0.094	almost significant
Wall Inner/Mid/Outer	30.87	2	15.44	1.006	0.403	not significant
State	43.17	2	21.58	1.407	0.294	not significant
Error	138.11	9	15.35	-		√15.35 = 3.92
Total	301.70	17	17.75			√17.75 = 4.21

7.5 Dynamic strain ageing

In Figure 7-9, tensile stress-strain curves are illustrated at x-y positions given by the inverted absolute temperature and the logarithmic strain rate used in each test. The test of AC-06 was interrupted accidentally. The collection of stress-strain curves shows that marked yield points are visible at low temperatures and that serrations in the stress-strain curves (flow curves) were present at medium temperatures, both observations demonstrating dynamic strain ageing. At higher temperatures, the yield points and the serrations in the flow curves disappear.

The maximum amplitude of the serrations for the present measurements occur at 250–275 °C. From their measurements of dynamic strain ageing Otterberg and Karlsson concludes that the strongest dynamic strain ageing occurs for low strain rates. Also, Ren et al. (2017) model a stronger dynamic strain ageing effect for strain rates of 10^{-5}/s. Surprisingly, as can be seen in Figure 7-9, the curves at the strain rate of 2×10^{-3} 1/s show the strongest strain ageing effect.

The ductility, measured as the elongation is listed in Table 7-12, for dynamic experiments. The data from Table 7-12, together with the static strain ageing data from Table 7-10, is plotted in Figure 7-10, and as can be seen, the ductility decreases after dynamic strain ageing, but retains relatively high values. The ductility is slightly lower in ST3 compared to ST1 already before strain ageing. Therefore, no difference in behaviour between the cylinders ST1 and ST3 could be detected after dynamic strain ageing.

Table 7-12. Elongations after dynamic strain ageing.

Specimen	State	Height	Wall	Elongation, A_5 (%)	Temperature (°C)	Strain rate (s^{-1})	Serration amplitude (N/mm^2)
ST1 AC-05	Stress-relieved	Bottom	Inner	26.2	220	0.002	70
ST1 AC-01	Annealed	Bottom	Inner	24.3	250	0.002	100
ST3 AC-11	Stress-relieved	Top	Mid	25.6	275	0.002	90
ST1 AC-10	As-received	Top	Mid	26.9	195	0.00025	20
ST3 AC-17	Stress-relieved	Bottom	Outer	22.1	220	0.00025	35
ST3 AC-14	As-received	Bottom	Outer	23.7	275	0.00025	20
ST3 AC-12	Annealed	Bottom	Outer	23.1	180	0.00007	20
ST1 AC-06	Stress-relieved	Bottom	Inner	24.6	255	0.00007	10
ST3 AC-08	As-received	Top	Mid	22.7	285	0.00007	10

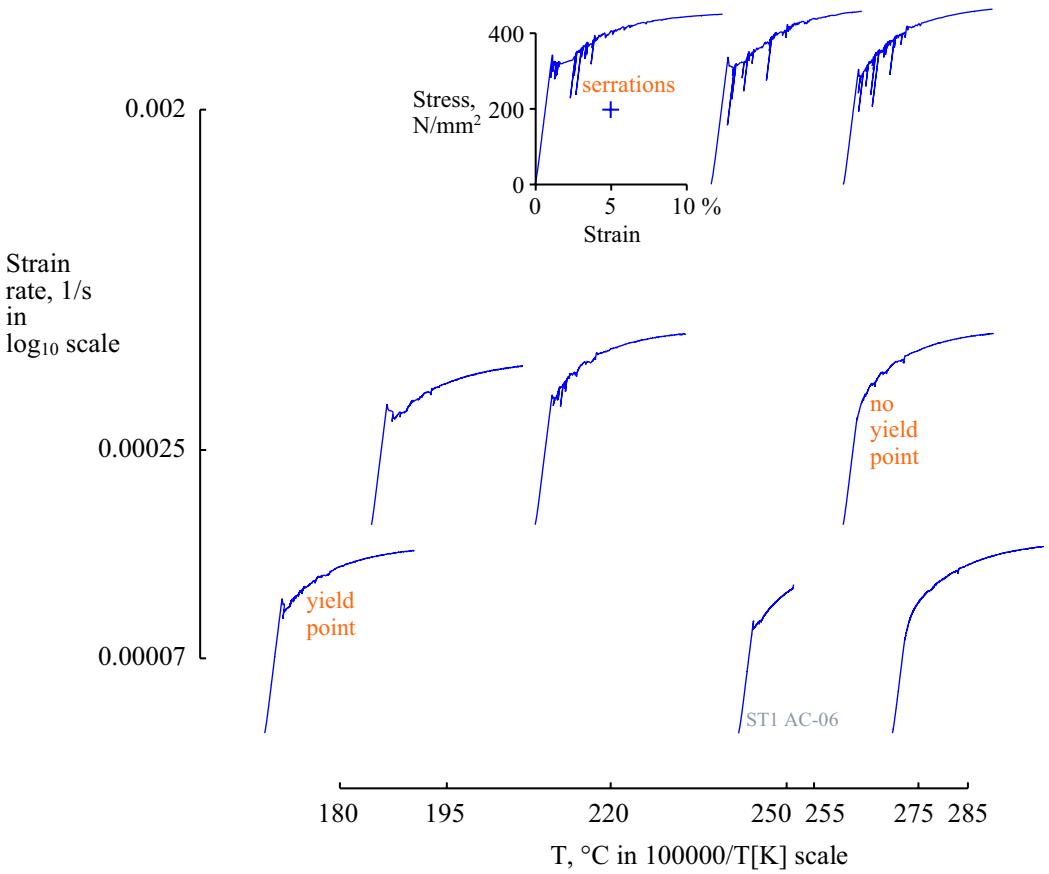

Figure 7-9. *Stress strain curves (in N/mm²) for the dynamic strain ageing experiments, plotted at the strain-rate versus inverse absolute temperature.*

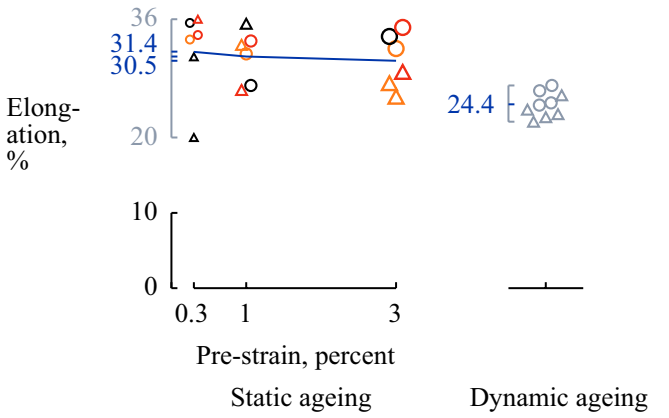

Figure 7-10. *Decrease in ductility after dynamic strain ageing compared to after static strain ageing.*

8 Discussion and conclusion

Strain ageing (UK English) or strain aging (US English) has been investigated thoroughly because of, among other things, its striking appearance during tensile testing at elevated temperatures and its importance for safety margins in reinforcement bars (Loporcaro et al. 2019) and nuclear reactor pressure vessels (Otterberg and Karlsson 1979, Murty and Charit 2008, Rao et al. 2021). Strain ageing has attracted researchers to theoretical reasoning and modelling of strain ageing deformation mechanics (Cottrell and Bilby 1949, Ren et al. 2017). The fundamental interaction of alloying elements with deformation structures in the crystal lattice (dislocations) is a key element in the understanding of strain ageing (Brindley and Barnby 1966, Cuddy and Leslie 1972).

The tensile strength of the tested steel cylinders seems to depend on the chemical composition of the ingot and this is supported by the difference of the microstructures in Figures 4-2 and 4-3, where ST1 appears to contain more ferrite than ST3. In addition, there seems to be a minor influence from the hot working process giving, for most test specimens, a slightly higher strength near inner and outer wall surfaces of the cylinders and slightly lower strength at mid sections. See Figure 3-2.

The steel cylinders all show an upper marked yield stress and elongation zone which are the signs of small atoms, as carbon and nitrogen, locking dislocations and thereby increasing the stress required for further deformation.

Tensile testing schemes to gain further knowledge of ageing of the steel components are presented in Section 6. The first testing scheme has been developed with consideration of the notion that dynamic strain ageing seems to occur in a certain temperature interval but also depends on the strain rate. The dynamic ageing seems to depend linearly on the inverse absolute temperature and the logarithm of the strain rate. The temperatures in the experimental design have been selected based on such dependencies and this might enhance the occurrence of dynamic strain ageing in the experiments. According to the experiments, dynamic strain ageing occurs for temperatures 180–300 °C. According to Otterberg and Karlsson (1979), dynamic strain ageing is not noticeable below 100 °C. Rao et al. (2021) shows that no dynamic strain ageing occurs below 150 °C. The ductility, measured as strain to fracture, decreases from 32 % after dynamic strain ageing, but remains relatively high at 24 %. As mentioned in Section 6, the temperature of the canister insert will peak initially at below 115 °C, and it will in the long term eventually decrease to the background temperature of the host rock of about 11 °C. Therefore, dynamic strain ageing is not likely to occur due to the low temperature.

The second testing scheme was developed with consideration of the notion that static strain ageing depend on the amount of pre-deformation. A series with logarithmic steps of pre-strain was selected in the design of the experiment in order to include both small and large deformations. From the strain ageing and tensile testing experiments in this report, it is clear that for ageing temperatures 20–155 °C, the pre-strain is the main influencing factor for strain ageing. Accounting for all data, irrespective of ageing time and temperature; for pre-strain 0.3 %, the strain ageing is negligible, for 1 % pre-strain, the rise in lower tensile strength is 10 N/mm^2, and for 3 % pre-strain, the increase in lower tensile strength is 80 N/mm^2. There seems to be a lower critical pre-strain, below which static strain ageing does not occur. The ductility is almost unaffected, for a pre-strain of 3 %, the elongation is on average around 30 %. The elongation decreased to 26 % for a single specimen at most.

Notwithstanding the marked, upper yield strength and a yield plateau of the steel cylinders, which shows that they display strain ageing, tensile testing show that they have good ductility of 30 % elongation and good toughness. This is interpreted as a good resilience to strain ageing for the steel cylinders.

Dymanic strain ageing of P355N steel is very apparent at 200–300 °C for a strain rate of 0.002/s. The ductility decreases slightly, but retains an elongation of 24 % in average. On the other hand, during a 5 cm shear load the temperature will only increase about 1 °C (SKB 2017) or 3 °C (Section 5 in this report) from a temperature 11–115 °C depending on the elapsed time after deposition of the canister. In mechanical analyses of the canister's resilience to shear loads in the repository, effects of dynamic strain ageing can be neglected based on the findings in the present report.

The requirement on the ductility is minimum 3 % for the canister insert (Jonsson et al. 2018), far below the standard values of 20 % (SS-EN 10216-3:2013). The insert material is therefore assessed to be able to strain age even without decreasing below that standard value. In mechanical analyses of the canister's resilience to shear loads in the repository, effects of static strain ageing can be neglected based on the findings in the present report. After experiencing a 5 cm shear load, the ductility measured as the elongation could change from around 34 % to 30 % due to static strain ageing, which can be considered negligible.

9 Acknowledgements

Element Materials Technology has performed the strain ageing tensile testing.

Swerea Swecast has contributed with the microstructural image in Figure 4-1.

Ylva Nilsson at YN Materialteknik has contributed with the microstructural images in Figures 4-2 and 4-3.

Allan Hedin has contributed with comments and formulation of conclusions. Staffan Larsson and Stefan Jonsson have reviewed and significantly improved the report. Anders Lindblom has suggested elaborations of the graphs. Professor emeritus Lars Holst has suggested and instructed the author in statistical methods. In addition, Lars has written the basic text in Section 7.1 together with the author.

Thanks for all the help.

Jan Sarnet

References

SKB's (Svensk Kärnbränslehantering AB) publications can be found at www.skb.com/publications. SKBdoc documents will be submitted upon request to document@skb.se.

Bergman B, 1992. Industriell försöksplanering och robust konstruktion. Lund: Studentlitteratur. (In Swedish.)

Bergman B, Arvidsson M, Gremyr I, 2017. Försöksplanering: för utveckling och förbättring. Lund: Studentlitteratur. (In Swedish.)

Bergström Y, Roberts W, 1971. The application of a dislocation model to dynamical strain ageing in α-iron containing interstitial atoms. Acta Metallurgica 19, 815–823.

Bhadeshia H K D H, Honeycombe R W K, 2017. Steels: microstructure and properties. Elsevier Science & Technology.

Björklund V, Hänninen H, Bossuyt S, 2024. Effects of static strain aging on mechanical performance of ductile cast iron. Journal of Materials Engineering and Performance. https://doi.org/10.1007/s11665-024-09716-9

Blom G, Holmquist B, 1998. Statistikteori med tillämpningar. 3. ed. Lund: Studentlitteratur. (In Swedish.)

Box G E P, Hunter J S, Hunter, W G, 2005. Statistics for experimenters: design, innovation and discovery. 2. ed. Hoboken, N.J.: Wiley-Interscience.

Brindley B J, Barnby J T, 1966. Dynamic strain ageing in mild steel. Acta Metallurgica 14, 1765–1780.

Caillard D, 2016. Dynamic strain ageing in iron alloys: The shielding effect of carbon. Acta Materialia 112, 273–284.

Cottrell A H, Bilby, B A, 1949. Dislocation theory of yielding and strain ageing of iron. Proceedings of the Physical Society 62A, 49–62.

Cuddy L J, Leslie W C, 1972. Some aspects of serrated yielding in substitutional solid solutions of iron. Acta Metallurgica 20, 1157–1167.

Dieter G E, 1988. Mechanical metallurgy. 3. ed. London: McGraw-Hill.

François D, Pineau A, Zaoui A, 1998. Mechanical behavior of materials Vol. 1 Elasticity and plasticity. Dordrecht: Kluwer.

Hensel A, Spittel T, 1978. Kraft- und Arbeitsbedarf bildsamer Formgebungsverfahren. Leipzig: VEB Deutscher Verlag für Grundstoffindustrie. (In German)

Honeycombe R W K, 1968. The plastic deformation of metals. London: Edward Arnold.

Hultgren A, 1966. Metallografins utveckling i Sverige under åren 1817–1966. Jernkontorets Annaler 150, 942–990. (In Swedish.)

Hultgren A, Selén A B, Öhman E, 1943. Värmebehandling av järn och stål. Uppsala: Svenska metallografförbundets förlag. (In Swedish.)

Hänninen H, Seifert H-P, Yagodzinsky Y, Ehrnstén O, Tarasenko O, Aaltonen P, 2001. Effects of dynamic strain ageing on environment assisted cracking of low alloy pressure vessel and piping steels. In: 10th Int. Conf. on Environmental Degradation of Materials in Nuclear Power Systems – Water Reactors, 6 – 10 August 2001, NACE/TMS/ANS, Lake Tahoe, Nevada, USA

Ikonen K, 2020. Temperatures inside SKB and Posiva type disposal canisters for spent fuel. Posiva SKB Report 12, Posiva Oy, Svensk Kärnbränslehantering AB.

Jana M, Dhar S, Acharyya S K, Chattopadhyay J, 2018. Effect of dynamic strain aging on tensile deformation of 20MnMoNi55 alloy. Journal of Materials Engineering and Performance 27, 6468–6478.

Jonsson M, Emilsson G, Emilsson L, 2018. Mechanical design analysis for the canister. Posiva SKB Report 04, Posiva Oy, Svensk Kärnbränslehantering AB.

Kocks U F, Argon A S, Ashby M F, 1975. Thermodynamics and kinetics of slip. Progress in materials science 19, 1–281.

Loporcaro G, Pampanin S, Kral M V, 2019. Long-term strain-ageing effects on low-carbon steel reinforcement. Construction and Building Materials 228, 116606.

Murty K L, Charit I, 2008. Static strain aging and dislocation–impurity interactions in irradiated mild steel. Journal of Nuclear Materials 382, 217–222.

Nilsson S, 2024. Dragprovning av deformationsåldrat stål P355N. Element Materials Technology AB. SKBdoc 2015753 ver 1.0, Svensk Kärnbränslehantering AB. (In Swedish.)

Otterberg R, Karlsson C, 1979. Åldring i svetsgods i reaktortryckkärl. IM-1358. Stockholm: Institutet för metallforskning. (In Swedish.)

Pihlajamäki T, 2017. Characterization of strain aging with full-field strain measurements. Masteruppsats. Aalto Universitet, Helsingfors.

Portevin A, Le Chatelier F, 1923. Sur un phénomène observé lors de l'essai de traction d'alliages en cours de transformation. Comptes rendus de l'Académie des sciences 176, 507–510. (In French)

Rao G S, Yagodzinskyy Y, Que Z, Spätig P, Seifert H-P, 2021. Study on hydrogen embrittlement and dynamic strain ageing on low-alloy reactor pressure vessel steels. Journal of nuclear materials 556, 153161.

Ren S, Mazière M, Forest S, Morgeneyer T F, Rousselier G, 2017. A constitutive model accounting for strain ageing effects on work-hardening. Application to a C-Mn steel. Comptes Rendus Mécanique 245, 908–921.

Renström P, 2020. Beräkningar av temperaturen i kopparhöljet och bufferten i förenklade parameterstudier. SKB R-19-27, Svensk Kärnbränslehantering AB. (In Swedish.)

Richardson G J, Hawkins D N, Sellars C M, 1985. Worked examples in metalworking. London: The Institute of Metals.

Rowe G W, 1977. Principles of industrial metalworking processes. London: Edward Arnold.

Sarnet J, 2022. Några mätningar av segjärns åldring. SKB R-22-04. Svensk Kärnbränslehantering AB. (In Swedish.)

Seifert H-P, Ritter S, 2005. Research and service experience with environmentally-assisted cracking in carbon and low-alloy steels in high temperature water. SKI Report 2005:60. Stockholm: Statens kärnkraftsinspektion.

Sekizawa M, 1981. The effect of stress relief heat treatment and strain aging on A737 grade C pressure vessel steel. Master's thesis, Lehigh University, Bethlehem, PA.

SKB, 2017. Svar till SSM på begäran om komplettering kring försprödningsmekanismer för kapseln. SKBdoc 1602500 ver 1.0, Svensk Kärnbränslehantering AB. (In Swedish.)

SS-EN 1563:2018. Gjutna material – Segjärn, Founding – Spheroidal graphite cast irons. Stockholm: Svenska institutet för standarder.

SS-EN 10216-3:2013. Seamless steel tubes for pressure purposes – Technical delivery conditions – Part 3: Alloy fine grain steel tubes. Stockholm: Swedish Standards Institute.

SS-EN ISO 6892-1:2019. Metallic materials – Tensile testing – Part 1: Method of test at room temperature. Stockholm: Swedish Standards Institute.

SS-EN ISO 6892-2:2018. Metallic materials – Tensile testing – Part 2: Method of test at elevated temperature. Stockholm: Swedish Standards Institute.

Tufte E, 1990. Envisioning Information. Cheshire, CT: Graphics Press.

Vater M, Heil H-P, 1971. Umformbedingungen und Gestaltung der Werkzeuge beim Freiformen. Stahl und Eisen 91, 864–876.

Wang H D, Berdin C, Mazière M, Forest S, Prioul C, Parrot A, Le-Delliou P, 2012. Experimental and numerical study of dynamic strain ageing and its relation to ductile fracture of a C-Mn steel. Materials Science and Engineering A 547, 19–31.

Wert C A, 1950. Measurements on the diffusion of interstitial atom in B.C.C. lattices. Journal of applied physics 21, 1196.

Zhao W, Chen M, Chen S, Qu J, 2012. Static strain aging behavior of an X100 pipeline steel. Materials Science and Engineering A 500, 418–422.

Appendix 1

Samples for strain ageing experiments

8 tensile samples were tested in as-received state, 11 samples in stress-relieved state 500 °C for 30 hours, 8 samples in subcritical process annealed state 650 °C for 4 hours. There were 13 tensile samples from ST1, 14 from ST3.

Table A1-1. Complete strain ageing tensile testing.

Run	Cylinder, specimen	Wall	Axial	State	Test	Temperature (°C)	Strain rate (s^{-1})	Time (h)	Strain (%)
103	ST1 AC-01	Inner	Bottom	Annealed	Dynamic	250	0.002		
106	ST3 AC-14	Outer	Bottom	As-received	Dynamic	275	0.00025		
108	ST3 AC-11	Mid	Top	Stress-relieved	Dynamic	275	0.002		
115	ST1 AC-05	Inner	Bottom	Stress-relieved	Dynamic	220	0.002		
117	ST3 AC-17	Outer	Bottom	Stress-relieved	Dynamic	220	0.00025		
118	ST1 AC-10	Mid	Top	As-received	Dynamic	195	0.00025		
119	ST1 AC-06	Inner	Bottom	Stress-relieved	Dynamic	255	0.00007		
120	ST3 AC-12	Outer	Bottom	Annealed	Dynamic	180	0.00007		
122	ST3 AC-08	Mid	Top	As-received	Dynamic	285	0.00007		
301	ST3 AC-07	Mid	Top	Annealed	Static	20		50	1
303	ST1 AC-03	Inner	Bottom	Stress relieved	Static	20		50	0.3
304	ST3 AC-10	Mid	Top	Stress relieved	Static	75		16	1
305	ST3 AC-09	Mid	Top	As-received	Static	155		5	1
308	ST1 AC-16	Outer	Bottom	Stress relieved	Static	155		50	1
309	ST1 AC-13	Outer	Bottom	Annealed	Static	155		16	3
312	ST1 AC-14	Outer	Bottom	Annealed	Static	20		5	1
313	ST1 AC-08	Mid	Top	Annealed	Static	75		50	3
314	ST3 AC-13	Outer	Bottom	Annealed	Static	20		5	0.3
316	ST3 AC-04	Inner	Bottom	Stress relieved	Static	155		5	3
317	ST1 AC-11	Mid	Top	As-received	Static	155		16	0.3
318	ST3 AC-01	Inner	Bottom	Annealed	Static	155		16	3
321	ST1 AC-04	Inner	Bottom	Stress relieved	Static	75		5	0.3
322	ST3 AC-15	Outer	Bottom	As-received	Static	75		50	0.3
323	ST3 AC-16	Outer	Bottom	Stress relieved	Static	20		16	0.3
324	ST3 AC-03	Inner	Bottom	As-received	Static	75		50	3
325	ST1 AC-12	Mid	Top	Stress relieved	Static	20		16	3
327	ST1 AC-02	Inner	Bottom	As-received	Static	75		5	1

Appendix 2

Specimen diameter

A2.1 Specimen diameter

According to Table 7-1 the diameters of the tensile specimens for the static strain-ageing tests vary. The possible influencing factors on the machined diameter were cylinder identity, radial position in cylinder wall, and top and bottom of the cylinder. From the averages in Table 7-1 and Figure 7-1, it is obvious that the diameters are larger for specimens from cylinder ST3 than from ST1. Specimens close to the inner wall of the cylinder also seem to be larger than specimens from the mid position or close to the outer wall.

Table A2-1. Measured diameters of tensile specimens from cylinders ST1 and ST3.

Tensile specimen diameter (mm)												
		Radial position in the cylinder wall										
Cylinder		Outer			Mid			Inner			Averages	
ST1	Top				13.988	13.979	13.995				13.9873	13.9877
	Bottom	13.986	13.992	13.955				13.988	14.007	13.999	13.9878	
ST3	Top				14.004	13.993	14.006				14.0010	14.0100
	Bottom	14.012	14.012	14.008				14.017	14.025	14.013	14.0145	
Averages		13.9942			13.9942			14.0082			13.9988	

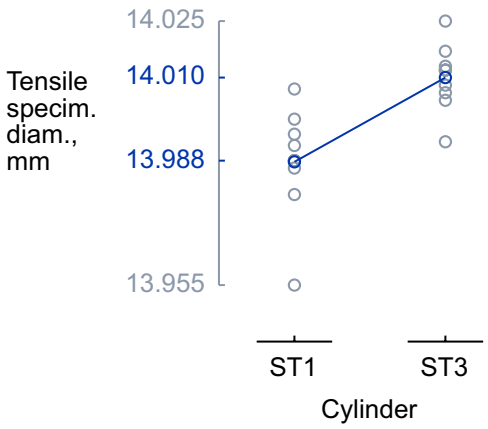

***Figure A2-1**. Measured tensile specimen diameters for the static strain ageing experiments.*

Systematic diameter differences between the cylinders (ST1/ST3) could be statistically ensured with Analysis of Variance, ANOVA, (Blom and Holmquist 1998, Box et al. 2005). Radial positions in the cylinder wall (Outer, mid, and inner) could almost be statistically ensured in the same analysis. In such variance analysis, the total squared variation around the mean value of the diameter, 0.00460 mm^2, is partitioned into components. According to the second column of Table 7-2, the analysis gave a partitioning into 4 components corresponding to cylinder, wall position, the interaction between cylinder and wall position, and a residual. The factor *Cylinder* has a statistically significant influence on the machined diameter and has been marked in red in Table 7-2. The diameter differs systematically between the cylinders ST1 or ST3. Contributions to the variation from other factors are included in the residual root mean square sum of 0.000107 mm^2 which gives an internal variation and standard deviation of 0.010 mm. Due to oversight of the author of this report, not all combinations of factors are represented in the tensile test specimens available in the design of the experiment. At each level of a factor, all levels of every other factor are not represented in Table 7-1 as they should in a proper Latin square design (sw. romerska kvadrater) (Box et al. 2005, pp 157–160, Bergman 1992, p 101). For example, at top (axial) cylinder position, no outer or inner wall samples have been withdrawn. Therefore, the variation between the bottom and top of the cylinder cannot be analysed.

Table A2-2. Analysis of Variance (ANOVA) table for tensile specimen diameters for the static strain ageing experiments.

Source of variation	Sum of squares	Degrees of Freedom	Mean squares	Ratio of mean square (F)	Significance probability (p)	Comment
Cylinder, ST1/ST3	0.00224	1	0.00224	21.00	0.000	(***) significant
Wall, Outer/mid/inner	0.00078	2	0.00039	3.67	0.057	almost significant
Height, Bottom/top		0				
Cylinder × Wall	0.00029	2	0.00014	1.35	0.295	not significant
Cylinder × Height		0				
Wall × Height		0				
Cylinder × Wall × Height		0				
Error	0.00128	12	0.000107			√0.000107 = 0.0103
Total	0.00460	17	0.000271			√0.000271 = 0.0165

The standard deviation √0.000107 = 0.0103 mm is a measure of variation after correcting for the influence of the cylinder, radial position in cylinder wall, and the interaction between the two. This variation has contributions both from the machining and measurement of the diameter. It could be a conservative measure of the accuracy in machining of the specimens, 0.0103/14.0 mm/mm = 0.07 %.

To highlight and describe variations in measurements, so-called normal distribution diagrams (plots) can be constructed and drawn. As an example, consider the tensile specimen diameters given to three decimal places for ST1 and ST3 in Table 7-3. First, the measured values are ordered by size and then the two variables y and z are calculated as indicated in Table 7-3 where Φ is the distribution function of the standard normal distribution (Blom and Holmquist 1998, pp 74–75, Box et al. 2005, pp 33–34). Instead of the classic calculation of the probability $y_i = (i-1/2)/n$ in those references, the present author calculates $y_i = (i-1/3)/(n+1/3)$ in line with the Statistica software.

Table A2-3. Measured diameters of tensile specimens from cylinders ST1 and ST3.

Number, i	Diameter tensile specimen ST1 (mm)	Diameter tensile specimen ST3 (mm)	$y_i = (i-1/3)/(n+1/3)$, $n = 9$	$z_i = \Phi^{-1}(y_i)$
1	13.955	13.993	0.071	−1.465
2	13.979	14.004	0.179	−0.921
3	13.986	14.006	0.286	−0.566
4	13.988	14.008	0.393	−0.272
5	13.988	14.012	0.5	0
6	13.992	14.012	0.607	0.272
7	13.995	14.013	0.714	0.566
8	13.999	14.017	0.821	0.921
9	14.007	14.025	0.929	1.465

The measurements x_i are plotted against $y_i = (i - 1/3)/(n + 1/3)$ and $z_i = \Phi^{-1}(y_i)$, $i = 1, 2, \ldots, n = 9$, as in Figure 7-2. The scale on the left vertical axis is linear in z. In Excel, z is calculated with the function NORM.S.INV. As can be seen, the plotted measurement points adhere well to straight lines, at least for specimens from cylinder ST3. This means that reasonable statistical descriptions and models for the variation within test cylinder ST3 is given by a normal distribution.

The arithmetic mean of the nine diameter measurements for ST1 is 13.988 mm and the standard deviation is 0.0147 mm. The corresponding numerical values for ST3 are 14.010 and 0.0089, respectively. The values determine the parameters in fitted normal distributions that become the ink blue lines in Figure 7-2. The two-sigma limits for the diameter of cylinder ST1 are 13.958 and 14.017, defining the normal distribution line. Similarly, two-sigma limits for ST3 are 13.992 and 14.028. The slopes of the lines are determined by the spread, standard deviation, within the sample positions, the smaller the spread, the steeper the slope. In Figure 7-2, the smallest specimen diameter at 13.955 mm from cylinder ST1 is an outlier of the distribution, and is even smaller than the lower two-sigma limit for ST1.

Although the order of the manufacturing of the tensile test specimens is not known, it can be reasoned from Figure 3-2 and Figure 7-2 that the higher tensile strength of ST3 seems to have led to a somewhat larger diameter of the specimens due to the resistance to (machining) deformation of the sample.

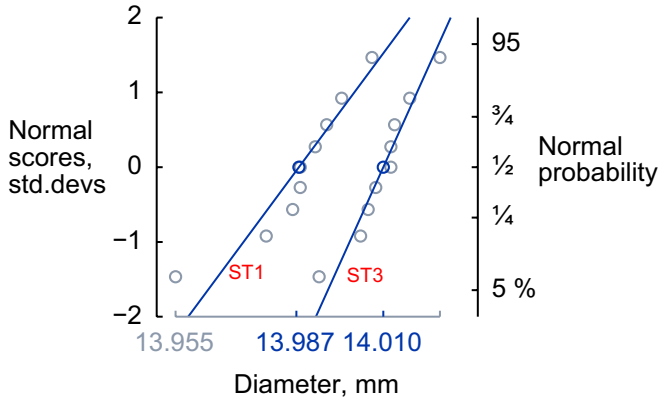

Figure A2-2. *Normal probability plots of the tensile specimen diameters from cylinders ST1 and ST3.*

Arkitektkopia AB, Bromma, 2024

SKB is responsible for managing spent nuclear fuel and radioactive waste produced by the Swedish nuclear power plants such that man and the environment are protected in the near and distant future.

skb.se